

NATIONAL AERONAUTICS AND SPACE ADMINISTRATION

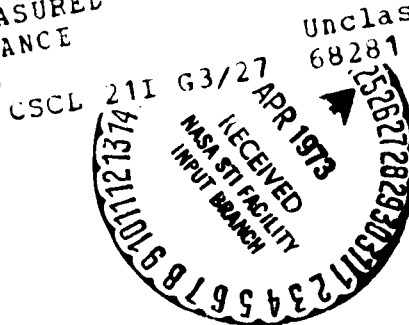
Technical Memorandum 33-548

*Simplified Procedures for Correlation of Experimentally
Measured and Predicted Thrust
Chamber Performance*

W. B. Powell

N73-21685

(NASA-CR-131519) SIMPLIFIED PROCEDURES
FOR CORRELATION OF EXPERIMENTALLY MEASURED
AND PREDICTED THRUST CHAMBER PERFORMANCE
(Jet Propulsion Lab.) 94 p HC \$0.75



**JET PROPULSION LABORATORY
CALIFORNIA INSTITUTE OF TECHNOLOGY
PASADENA, CALIFORNIA**

April 1, 1973

NATIONAL AERONAUTICS AND SPACE ADMINISTRATION

Technical Memorandum 33-548

*Simplified Procedures for Correlation of Experimentally
Measured and Predicted Thrust
Chamber Performance*

W. B. Powell

**JET PROPULSION LABORATORY
CALIFORNIA INSTITUTE OF TECHNOLOGY
PASADENA, CALIFORNIA**

April 1, 1973

Prepared Under Contract No. NAS 7-100
National Aeronautics and Space Administration

PREFACE

The work described in this report was performed by the Propulsion Division of the Jet Propulsion Laboratory.

CONTENTS

I. Introduction	1
II. JANNAF Performance Prediction Methodology	4
III. Experimental Measurements and Specification of Operating Conditions	9
IV. Experimental Determination of Vacuum Specific Impulse	10
V. Simplified Form for Analytical Prediction of Vacuum Specific Impulse	12
VI. Correlation of Experimentally Measured and Predicted Vacuum Specific Impulse	27
VII. Performance Prediction for Related Thrust Chamber Configuration	30
VIII. Experimental Determination of Characteristic Velocity	30
IX. Simplified Form for Analytical Prediction of Characteristic Velocity	34
X. Correlation of Experimentally Measured and Predicted Characteristic Velocity and Comparison With Specific Impulse Parameters	39
Appendix A. Boundary-Layer Effects on Performance	53
Appendix B. Flox-MMH Propellant Data	63
Appendix C. Example Correlation and Extrapolation of Flox-MMH Test Data	71
Appendix D. Correction of ODE Performance for Change in Propellant Injection Temperature	76
Appendix E. Calculation of Injector Region Heat Loss Effects	79
Nomenclature	83
References	87
TABLES	
1. Thrust chamber performance losses	42
2. Thrust chamber performance computer programs	42

PRECEDING PAGE BLANK NOT FILMED

CONTENTS (contd)

TABLES (contd)

3.	Development of approximate method for predicting vacuum specific impulse	43
4.	Development of approximate method for predicting characteristic velocity	44
B-1.	Recommended heats of formation for propellants	65
C-1.	Test data and efficiency factor correlation for tests of 600-lbf Flox (88-12)-MMH thrust chamber with $\epsilon = 2.5$ nozzle area ratio and extrapolation to performance at $\epsilon = 60$ nozzle area ratio	75

FIGURES

1.	Simplified performance prediction and correlation procedure chart	45
2.	Internal processes in the real rocket thrust chamber	46
3.	Experimental data needed for thrust chamber performance and evaluation	46
4.	Effect on performance of heat losses from interior of thrust chamber	47
5.	Two-dimensional specific impulse efficiency for conical nozzles at $\gamma = 1.20$	48
6.	Two-dimensional specific impulse efficiency for conical nozzles at $\gamma = 1.32$	48
7.	Typical effect of throat wall radius of curvature on the two-dimensional specific impulse efficiency of conical nozzles	49
8.	Effect of combustion chamber area ratio on chamber static pressure at injection end and downstream end of cylindrical combustion chamber	50
9.	Effect of nozzle throat radius of curvature on two-dimensional nozzle flow coefficient	51
10.	Explanation of data shown in Fig. 9	52
A-1.	Boundary-layer parameter definitions	60
A-2.	Effect of boundary layer on nozzle geometry	60

CONTENTS (contd)

FIGURES (contd)

A-3.	Perfect gas values of the thermodynamic function $[\epsilon(p_e/p_0^*)(\rho_e u_e^2/p_e)]$ used in calculating performance loss due to boundary-layer effects	61
A-4.	Perfect gas values of the thermodynamic function $(\rho_e u_e^2/p_e)$ used in calculating performance loss due to boundary-layer effects	62
B-1.	ODE reference performance for Flox (88-12)-MMH (enthalpy, chamber temperature, characteristic velocity)	66
B-2.	ODE reference performance for Flox (88-12)-MMH (vacuum specific impulse vs nozzle area ratio)	67
B-3.	Kinetic efficiency factors for Flox (88-12)-MMH	68
B-4.	Effect of injection enthalpy change on performance of Flox (88-12)-MMH	69
B-5.	Boundary-layer loss estimate for 600-lbf thrust chamber	70
E-1.	Experimental thrust chamber configuration	82

ABSTRACT

Thrust chamber performance should be evaluated in terms of an analytical model incorporating all the loss processes that occur in a real rocket motor. The Performance Standardization Working Group of JANNAF has identified the important loss processes in the real thrust chamber, and has developed a methodology and a recommended procedure for predicting real thrust chamber vacuum specific impulse.

Simplified equations, based on the JANNAF reference procedure for calculating vacuum specific impulse, are developed to relate the delivered performance (both vacuum specific impulse and characteristic velocity) to the ideal performance as degraded by the losses corresponding to a specified list of loss processes. These simplified equations enable the various performance loss components, and the corresponding efficiencies, to be quantified separately (except that interaction effects are necessarily arbitrarily assigned in the process).

The loss and efficiency expressions presented can be used to evaluate experimentally measured thrust chamber performance, to direct development effort into the areas most likely to yield improvements in performance, and as a basis to predict performance of related thrust chamber configurations.

I. INTRODUCTION

The JANNAF Performance Standardization Working Group started work in 1965, and in 1968 published the ICRPG Liquid Propellant Thrust Chamber Performance Evaluation Manual (Ref. 1) and several related reports. The manual presented a basic physical model for the rocket thrust chamber, including a listing of the primary loss processes, and described the methodology and computer programs which were available at that time for computing thrust chamber performance.

Since 1968, the Working Group has continued to refine the methodology and the capabilities of the computer programs. In particular, an earlier empirical approximation used to describe the energy release loss is being replaced by a model based on physically describable processes. New computer programs have also been developed to implement the improvements in the methodology.

New and revised manuals describing the improved performance prediction methodology and its application to correlation and analysis of measured thrust chamber performance are in the process of preparation and adoption by the Performance Standardization Working Group, but will probably not be published and distributed until some time in 1973.

This report describes approximate procedures that can be used to correlate and evaluate experimentally measured thrust chamber performance during the period between the general acceptance of the improvements in the methodology by those working in the field and the publication of formally accepted manuals describing the improvements and their application. The approximate procedures described here are completely consistent with the physical model and the loss process descriptions currently envisioned for the revised JANNAF reference methodology (see next section).

Two rocket motor performance parameters are considered. The vacuum specific impulse $I_{sp_{vac}}$ is the thrust per unit mass flow of propellant. This parameter directly determines the performance and payload of a rocket-propelled vehicle. The vacuum specific impulse must be measured or predicted with the highest possible accuracy; the current goal is $\pm 1\%$ for new propellants and conditions, and even closer prediction for well-characterized systems. Both the experimental measurements and the analytical techniques used in evaluating the vacuum specific impulse are capable of achieving this accuracy goal in most instances.

The characteristic velocity c^* is a mass flow parameter. It is used both to predict mass flow (which, in conjunction with the vacuum specific impulse, determines thrust level) and to obtain the preliminary estimation of the effect of the various loss processes on performance. (Note that the effect of a given loss process on characteristic velocity is not exactly the same as its effect on vacuum specific impulse.) The characteristic velocity can be determined experimentally by testing a motor having a low exit-area-ratio exhaust nozzle; thrust measurement is not required. Experimental determination of c^* is generally less accurate than I_{sp} (about ± 2 or 3% uncertainty) because of various measurement and data correction problems and assumptions involved in the definition of this parameter. An accuracy of ± 2 or 3% is considered satisfactory for design purposes, since mass flow rates can usually be adjusted by this amount to obtain a desired thrust level in a vehicle. Both the vacuum specific impulse and characteristic velocity are relatively insensitive to small changes in the level of the chamber pressure at which they are evaluated.

Vacuum specific impulse is the preferred parameter for performance evaluation and correlation, because specific impulse is more meaningful and can be determined with better accuracy than the characteristic velocity.

The analytical model employed for predicting thrust chamber performance can be used to show the effect on the potentially achievable performance of each of the included loss processes. This capability is useful during rocket engine development, as it enables the magnitude and acceptability of individual loss components to be evaluated and thus shows where further development work would be profitable.

As a first principle, experimental performance is to be stated as of the conditions under which it is measured and the reference ideal performance calculated to correspond to the specified test conditions before comparison with the test data.

In using the approximate methods of performance prediction, all eight of the losses and effects listed in the next section must be considered and accounted for. (Note that any unknown or unaccounted-for losses or effects will be forced to appear as part of one of the recognized losses during the correlation process.) In addition, it must be recognized that the approximate methods result in an arbitrary distribution of the interaction effects among the various losses.

Five primary steps are involved in the analytical correlation and evaluation of experimentally measured thrust chamber performance (see Fig. 1):

- (1) Determination of the experimental performance parameters for the actual operating conditions, based on specific measured data and on appropriate corrections to the measured data.
- (2) Specification of the conditions under which the experimental performance has been obtained.
- (3) Calculation of the analytically predicted performance corresponding to the specified test conditions, with the implicit determination of the magnitude of all losses.
- (4) Comparison of experimental and predicted performances. The predicted and the experimentally measured performances are compared to see if they are in acceptable agreement. The agreement criteria will depend upon the uncertainty associated with both the predicted and the measured performances; but agreement to within $\pm 1\%$ is the desired goal. If acceptable agreement is not achieved initially, the test measurements, input data, modeling, and calculations must be reviewed and errors found and corrected.¹ This process must be repeated until acceptable

¹The reference thrust chamber performance model can be changed only by action of the full JANNAF Performance Standardization Working Group.

agreement (correlation) is achieved. It is then presumed that the loss magnitude and efficiencies associated with the correlated performance prediction are a correct representation of the losses occurring in the experimental thrust chamber.

- (5) Evaluation of performance and losses. The overall performance, the overall performance efficiency, and the individual losses and their corresponding efficiencies are evaluated to determine whether they are acceptable, or whether improvement in any area appears feasible with the state-of-the-art. At this point, a decision is made to continue development or to accept the thrust chamber design and performance at its existing stage of development.

The correlation and evaluation procedure described above, and charted in Fig. 1, serves as confirmation of the satisfactory completion of a thrust chamber development program, or as a guide in determining the areas where further development work needs to be done.

II. JANNAF PERFORMANCE PREDICTION METHODOLOGY

The JANNAF performance prediction methodology currently enables calculation of steady-state vacuum specific impulse

$$I_{sp} \\ \text{vac} \\ \text{pred}$$

of liquid-liquid propellant injection thrust chambers which (1) have only gaseous combustion products, (2) have conventional de-Laval nozzles, and (3) are large enough that the boundary layer influences only a small part of the total flow. The methodology takes into account the following interacting losses, with reference to one-dimensional isentropic equilibrium flow performance as ideal:

- (1) Energy-release loss, consisting of two parts:
 - (a) Vaporization loss — due to incomplete liquid droplet vaporization at the nozzle throat, including thrust effects

due to both reacted gas and remaining liquid droplet components.

- (b) Mixture-ratio distribution loss — due to macroscopic non-uniform lateral distribution of the local time-averaged mixture ratio of vaporized propellant at the nozzle throat.²
- (2) Kinetic loss — due to rate-limited equilibrium shift during expansion.
- (3) Two-dimensional loss — due to upstream nozzle throat curvature (which affects only mass flow and, hence, c^*), and to nozzle divergence shape and exit angle (which affect only the vacuum specific impulse).
- (4) Boundary-layer loss — due to friction and heat transfer at the wall.

Within the context of, or as input to, the computer programs used in the methodology, it is possible to account for effects due to

- (5) Propellant impurities. (Adjust enthalpy and composition of injected propellant.)
- (6) Heat lost to the thrust chamber from the injector face and the chamber wall upstream of the boundary-layer attachment point.³ (Reduce enthalpy of injected propellants.)

²There can be an additional mixture-ratio distribution loss due to timewise variations from the mean in the mixture ratio of the vaporized propellant flowing through any element of the nozzle throat cross section. This temporal component of the mixture-ratio distribution loss is not presently accounted for in the JANNAF methodology.

³In some rocket motors, there is a turbulent region just downstream from the injector, followed by a region in which the boundary layer appears to develop normally. Heat transfer upstream of the effective starting point for the boundary layer and radiant heat transfer throughout the thrust chamber must be accounted for separately from the boundary-layer calculations. The location of the effective starting point for the boundary layer is determined experimentally by examination of the axial variation of the wall heat flux.

- (7) Mass addition into boundary layer. (Use MABL or BLIMP programs.)⁴
- (8) Feed-system energy loss and exchange, such as that due to pumps, turbines, and regenerative-cooling heat transfer. (Adjust enthalpy of injected propellants.)

In order to develop the analytical expressions for predicting the delivered performance, the real rocket thrust chamber is modeled as a number of inviscid stream tubes flowing within a virtual nozzle. The virtual nozzle is offset from the real nozzle wall by a distance δ^* , obtained from the boundary-layer analysis, such that the mass flux of the real and the inviscid flows is identical (Fig. 2). There is no mixing across stream-tube boundaries.

The stream tubes are constrained to flow together through the throat of the virtual nozzle. The individual and the total stream-tube mass flow are related to the throat size and curvature, and to the pressure level in the combustion chamber.

The thrust chamber vacuum specific impulse

$$I_{sp}^{\text{vac pred}}$$

is obtained by summing the thrust of the equivalent inviscid-flow stream tubes and adding corrections for the pressure force and the momentum deficiency of the flow in the boundary layer at the nozzle exit, and dividing by the discharged mass flow rate.

For liquid-liquid spray injection, the composition of the gases flowing through the stream tubes is given by a distributed energy-release combustion model (DER), which assumes that droplet distribution from the injection elements establishes the stream-tube configuration and that droplet evaporation is the controlling factor in the combustion energy-release process. Thus, a stream tube contains at any location a quantity of completely reacted

⁴Mass addition boundary-layer programs being developed by the JANNAF Performance Standardization Working Group.

gas and a residual of unevaporated liquid droplets; the mixture ratio of the evaporated and reacted combustion gas may differ from the initial injected mixture ratio of the stream tube.

The basic JANNAF performance prediction methodology computes vacuum specific impulse by the following procedure:

- (1) The distributed energy-release series of computer programs is used to compute the vaporized (and reacted) mass, mixture-ratio, enthalpy, and stagnation pressure (or entropy) distributions of the flow at the nozzle throat. Input to this program is basically the injected propellant mass, enthalpy, mixture-ratio, and droplet-size distributions.
- (2) The TDK program uses the output of the DER program to compute the two-dimensional kinetic multi-stream-tube inviscid-flow nozzle performance. This initial calculation, TDK1, is made with the geometric nozzle dimensions, in order to obtain boundary stream-tube properties that can be used to compute boundary-layer parameters.⁵
- (3) A boundary-layer program, either an integral-method program such as TBL or a finite-difference-type program such as MABL or BLIMP, is used to compute the boundary-layer momentum and displacement thickness, using input data from the TDK program.
- (4) A final TDK calculation, TDK2, is made using the virtual nozzle dimensions, to obtain the inviscid gas-flow thrust and the properties of the boundary stream-tube flow at the nozzle exit.

⁵Note that TDK is a package of programs which also contains the one-dimensional equilibrium program ODE, the one-dimensional kinetic program ODK, a transonic program TRANS, and a TDE option. A two-dimensional equilibrium program TDE may be added to the programs available, either separately or as an option in the TDK program package. TDE may be useful as a less-expensive substitute for TDK in obtaining boundary stream-tube properties for computing boundary-layer parameters.

- (5) The total thrust is the sum of
- (a) The thrust resulting from the inviscid kinetic expansion of the throat-plane vaporized and reacted gases through the effective supersonic nozzle contour (from TDK2).
 - (b) The momentum flux of the unevaporated liquid droplets passing through the nozzle throat plane (from DER).
 - (c) The thrust deficiency of the real gas flow, with its boundary layer, compared to the assumed inviscid flow (from TBL, etc., and TDK2).

At present the assumption is made that interaction of the already-combusted gases with the remaining liquid droplets (momentum exchange, evaporation, energy release) downstream of the throat plane has no net effect on the thrust as given by items (5)(a), (b), and (c), above. The performance losses and the computer programs used in calculating performance are summarized in Tables 1 and 2.

Modifications and extensions to the methodology to enable prediction of performance with gas-liquid and gas-gas propellant injection are currently being considered, and at some time in the future it is anticipated that provisions will be made to handle 2-phase combustion products.

It is important to recognize that, at the present stage of development of the JANNAF performance evaluation procedures, only loss mechanisms (1) through (8), above, are considered. Meaningful correlation and evaluation of experimental data can be achieved only when the comparison analytical model incorporates all of the loss processes present in the real motor being evaluated. Fortunately, the losses (1 through 8) inventoried are adequate to model most currently important thrust chamber configurations. Thus, the JANNAF methodology serves a useful purpose in its present state of development, even while steps are being taken to extend it to cover more complicated systems.⁶

⁶The computer programs ODE, ODK, TDK, TBL, and MABL can be obtained from CPIA, 9261 Georgia Ave., Silver Spring, Maryland 20910 (Attn: Tom Reedy). The computer program DER, in a version which handles both liquid-liquid and gas-liquid injection, has been developed by Rocketdyne for JPL under Contract NAS 7-746, and is currently being checked by JPL. In its current form, DER does not appear to model

III. EXPERIMENTAL MEASUREMENTS AND SPECIFICATION OF OPERATING CONDITIONS

If experimentally measured and predicted thrust chamber performances are to be correlated, it is necessary that all of the required measurements be made to enable determination of the experimental performance and that the conditions under which the performance is measured be completely specified, so that the corresponding performance prediction can be made.

The experimental data, which are required to determine delivered values of vacuum specific impulse and characteristic velocity or as input to the performance prediction procedure and which must be measured during thrust chamber operation, are listed below and indicated in Fig. 3:

F_{amb}	measured thrust
\dot{m}_o, \dot{m}_f	propellant flow rates, oxidizer and fuel
T, p	propellant temperature and pressure, oxidizer and fuel, at injector inlet
A_t, A_e, A_{lip}	nozzle throat, exit, and lip areas (Since it is difficult to measure these during motor operation, corrected "cold" measurements are usually used.)
P_s	static pressure at a specified axial location and chamber area ratio
P_a	ambient pressure
P_{lip}	"base pressure" at nozzle lip
T_w, q_w	temperature and heat flux profiles at chamber and nozzle wall (Measured values are desirable, though these quantities can be calculated.)

adequately the gas-liquid injection case, and improvement will have to await results of fundamental studies in this area. It is expected that the existing DER program will become available through COSMIC or CPIA by March 1973. Improved versions of DER will print out interface information needed to start the TDK calculation, and both DER and TDK will print out information needed to start boundary-layer calculations with TBL, MABL, or BLIMP. BLIMP is an alternate boundary-layer program which is currently being modified to fit into the JANNAF family of programs.

Additional information, beyond the data which must be obtained during testing, is needed as input for the performance prediction computer programs and procedures, and for the calculation of the experimental delivered performance. This information falls into three general categories:

- (1) Chamber and nozzle size and shape, including:
 - (a) Chamber diameter and length.
 - (b) Location and area ratio at chamber static pressure taps.
 - (c) Throat radius of curvature.
 - (d) Nozzle throat area, exit area, and lip area. ("Cold" measurements should be corrected for thermal and pressure effects to obtain effective "operational" values.)
- (2) Propellant inlet conditions:
 - (a) Composition, including impurities.
 - (b) Enthalpy, including any effects due to regenerative cooling and impurities.
- (3) Propellant injection characteristics: mass, mixture ratio, drop size, and enthalpy distribution.

IV. EXPERIMENTAL DETERMINATION OF VACUUM SPECIFIC IMPULSE

Vacuum specific impulse can be determined directly from tests made in a vacuum environment, or it can be calculated from measurements made during test of a low-area-ratio configuration (fully attached nozzle flow) thrust chamber in an ambient pressure environment. The physical and geometrical data, which are required both to determine the experimental value of the vacuum specific impulse and to define the corresponding analytical model, are listed in the preceding section.

The general expression for the experimentally measured thrust chamber vacuum specific impulse is

$$I_{sp \text{ vac exp}} = \frac{F_{amb} + p_a A_e + \int (p_a - p_{lip}) dA_{lip}}{\dot{m}_t} \quad (1)$$

This expression includes corrections for the external pressure effect on the lip thickness of the real nozzle, a factor which, while usually small, should not be neglected. The quantities are defined in Fig. 3.⁷

At this point, it is convenient to define an overall thrust chamber specific impulse efficiency

$$\eta_{I_{sp \text{ TC exp}}} = \frac{I_{sp \text{ vac exp}}}{I_{sp \text{ vac ODE (O/F)avg}}} \quad (2)$$

⁷ An overall specific impulse for an entire engine assembly can be defined as

$$I_{sp \text{ engine}} = \frac{\Sigma F}{\Sigma(\text{mass discharged})}$$

- where
- (1) ΣF includes all thrust contributions, from the main thrust chamber and from other sources, such as turbine exhausts and separately exhausted coolant flows.
 - (2) $\Sigma(\text{mass discharged})$ includes the mass discharged from the main thrust chamber, that discharged from auxiliary propulsive dumps, and that which is vented or leaks from any part of the system whether or not it produces any net thrust.

This report deals only with the thrust chamber performance parameters, and does not consider "external" effects associated with feed systems, pumps, turbine exhausts, vents, or thrust chamber coolant flows which are expanded and discharged separately from the combustion chamber gases. Any references to "system" within this report refer only to the thrust chamber and its regenerative cooling flows, if any.

where

$$I_{sp \text{ vac ODE (O/F)avg}}$$

is the ideal thrust chamber performance that would be attained in the absence of all of the real thrust chamber internal loss processes. It is calculated using the ODE computer program for the actual thrust chamber test injector-inlet propellant composition and enthalpy, and nozzle exit-area ratio. Note that, for a regeneratively cooled chamber, the injector-inlet propellant enthalpy must include the heat transferred to the propellant from the chamber, and is not the propellant enthalpy at the thrust chamber inlet.

V. SIMPLIFIED FORM FOR ANALYTICAL PREDICTION OF VACUUM SPECIFIC IMPULSE

A close analytical approximation to the JANNAF reference procedure for calculating thrust chamber specific impulse is

$$I_{sp \text{ vac pred}} = \sum I_{sp_i \text{ vac TDK (O/F)_{i,vap}^* HL \epsilon' \text{ drop interact}}} \left(\frac{\dot{m}_{i,vap}^*}{\dot{m}_t} \right) - \frac{\Delta_1 F_{BL}}{\dot{m}_t} + \frac{\Delta F_{drops}}{\dot{m}_t} \quad (3)$$

where

- (1) $\dot{m}_{i,vap}^*$ and $(O/F)_{i,vap}^*$ are stream-tube evaporated mass and mixture ratio at the throat.
- (2) $\Delta_1 F_{BL}$ is a thrust decrement which accounts for friction and heat-transfer effects in the boundary layer, based on flow through the equivalent inviscid-flow nozzle of area ratio ϵ' .
- (3) ΔF_{drops} is a thrust increment equal to the momentum flux of the liquid droplets passing through the throat plane of the nozzle.

- (4) The subscript HL indicates that the enthalpy of the propellant at the injector inlet H_{inj} has been reduced to account for heat loss in addition to that accounted for by the boundary-layer computer program (TBL, MABL, or BLIMP). The additional heat losses for which correction should be made are
- (a) Heat lost to the system by convective or radiative heat transfer in the region upstream of the turbulent boundary-layer start point. This heat can be stored in the thrust chamber wall, lost to the outside environment by convection or radiation, or picked up by a regenerative coolant in such a manner that the measured propellant enthalpy at the injector inlet is increased. (Heat which is picked up by the propellant but does not increase measured enthalpy at the injector inlet, for instance heat recycled from the injector face plate, does not enter into this correction.)
 - (b) Heat losses due to radiation from the combustion gases to the chamber and nozzle walls in the turbulent boundary layer region, and, in the divergent portion of the nozzle, the heat lost by direct radiation from the gases to the outside environment.
- (5) The subscript ϵ' indicates that the quantities are determined for an equivalent inviscid-flow nozzle, obtained by displacing the boundary of the real nozzle by the displacement thickness of the boundary layer δ^* .
- (6) The subscript "drop interact" indicates that the enthalpy of the vaporized propellant has been reduced to account for the energy used to accelerate the liquid droplets remaining at the nozzle throat.

The radiative heat loss from the nozzle-exit section can be significant for some small thrust chambers, but no standard method of accounting for this loss has been developed, and it is not considered further in this paper.

Heat radiated to the inside walls of the thrust chamber can be treated as an addition to the convective heat transfer (as far as total heat loss and heat balance are concerned) in both the region upstream of the turbulent

boundary-layer start point and in the turbulent boundary-layer region itself, but will not enter into the calculation of the boundary-layer displacement and momentum thicknesses other than as it increases the temperature of the inside surface of the combustion chamber.

The various heat losses and their corresponding treatment in the performance prediction procedure are indicated in Fig. 4.

The droplet thrust term will be ignored from here on in the development and discussion of the simplified performance prediction procedure. This can be justified by the following arguments:

- (1) In any acceptable rocket motor, the unevaporated propellant droplet fraction will be small, and the major part of the residual droplet effect will show up in the decreased mass of the reacted product gases.
- (2) The thrust of the droplets at the throat plane arises from entrainment in and momentum transfer with the surrounding reacted gases, with a corresponding slowing down of the gases. For small droplet fractions, it is reasonable to offset the throat momentum flux of the droplets against the associated slowing down of the gases at the throat. This is effectively accomplished by using the existing computer programs (ODE, ODK, and TDK) with the as-injected propellant enthalpy to calculate the reacted gas properties and performance, and omitting the droplet thrust term.

Equation (3) can now be replaced by Eq. (4), where the stream-tube performance is calculated for single-phase gas flow through the equivalent inviscid-flow nozzle, the droplet thrust term has been omitted, and the boundary-layer term has been expanded in terms of the boundary-layer

parameters θ_e and δ_e^* and the gas properties in the boundary-layer stream tube at the exit station of the equivalent inviscid-flow nozzle:⁸

$$I_{sp \text{ pred}} = \sum_{\substack{\text{TDK} \\ \text{(O/F)}_{i, \text{vap}}^* \\ \text{HL} \\ \epsilon'}} I_{sp_i} \left(\frac{\dot{m}_{i, \text{vap}}^*}{\dot{m}_t} \right) - \left\{ \frac{2p_e A_e \cos \alpha_e}{\dot{m}_t} \left[\left(\frac{\rho_e u_e^2}{p_e} \right) \left(\frac{\theta_e}{r_e} \right) - \left(\frac{\delta_e^*}{r_e} \right) \right] \right\}_{\substack{\text{TDK} \\ \epsilon'}} \quad (4)$$

Additionally, the subscript "vac" has been dropped, and it is from here on to be understood that specific impulse is always calculated for vacuum conditions.

It is desirable that a simplified performance prediction calculation procedure be referenced to the real nozzle exit-area ratio and dimensions. The exit-area ratio of the real and of the equivalent inviscid-flow nozzles are related by the expression

$$(\epsilon' - \epsilon) = -2\epsilon \frac{\left[\left(\frac{\delta_e^*}{r_e} \right) \cos \alpha_e - \left(\frac{\delta_t^*}{r_t} \right) \right]}{\left(1 - 2 \frac{\delta_t^*}{r_t} \right)} \quad (5)$$

Now Eq. (4) can be put in the form

$$I_{sp \text{ pred}} = \sum_{\substack{\text{TDK} \\ \text{(O/F)}_{i, \text{vap}}^* \\ \text{HL} \\ \epsilon'}} I_{sp_i} \left(\frac{\dot{m}_{i, \text{vap}}^*}{\dot{m}_t} \right) + \frac{\partial}{\partial \epsilon} \left[\sum_{\substack{\text{TDK} \\ \text{(O/F)}_{i, \text{vap}}^* \\ \text{HL} \\ \epsilon'}} I_{sp_i} \left(\frac{\dot{m}_{i, \text{vap}}^*}{\dot{m}_t} \right) \right] (\epsilon' - \epsilon) \\ - \left\{ \frac{2p_e A_e \cos \alpha_e}{\dot{m}_t} \left[\left(\frac{\rho_e u_e^2}{p_e} \right) \left(\frac{\theta_e}{r_e} \right) - \left(\frac{\delta_e^*}{r_e} \right) \right] \right\}_{\substack{\text{TDK} \\ \epsilon}} \\ - \frac{\partial}{\partial \epsilon} \left\{ \frac{2p_e A_e \cos \alpha_e}{\dot{m}_t} \left[\left(\frac{\rho_e u_e^2}{p_e} \right) \left(\frac{\theta_e}{r_e} \right) - \left(\frac{\delta_e^*}{r_e} \right) \right] \right\}_{\substack{\text{TDK} \\ \epsilon}} (\epsilon' - \epsilon) \quad (6)$$

⁸The boundary-layer parameters θ_e and δ_e^* are defined and discussed in Appendix A.

From this point on all quantities will be evaluated at the geometrical nozzle exit-area ratio ϵ . The fluid properties in the last two terms of Eq. (6), (ρ_e , u_e , and p_e) are understood to be evaluated at the edge of the equivalent inviscid flow at the exit plane of the nozzle (TDK).

Since the second term of Eq. (6) is a change in thrust associated with a change in nozzle exit-area ratio caused by the boundary layer, this term is combined with the third and fourth terms as the total boundary-layer effect on specific impulse, $\Delta_2 I_{sp_{BL}}$, to be used when specific impulse is referenced to the value corresponding to inviscid flow through the geometrical nozzle.

The predicted specific impulse is then given by

$$I_{sp_{pred}} = \sum_{\substack{\text{TDK} \\ (\text{O/F})_{i,vap}^* \\ \text{HL} \\ \epsilon}} I_{sp_i} \left(\frac{\dot{m}_{i,vap}^*}{\dot{m}_t} \right) - \Delta_2 I_{sp_{BL}} \quad (7)$$

where

$$\begin{aligned} \Delta_2 I_{sp_{BL}} = & \left\{ \frac{2A_e p_e \cos \alpha_e}{\dot{m}_t} \left[\left(\frac{\rho_e u_e^2}{p_e} \right) \left(\frac{\theta_e}{r_e} \right) - \left(\frac{\delta_e^*}{r_e} \right) \right] \right\}_{\substack{\text{TDK} \\ \epsilon}} \\ & + \frac{\partial}{\partial \epsilon} \left\{ \frac{2A_e p_e \cos \alpha_e}{\dot{m}_t} \left[\left(\frac{\rho_e u_e^2}{p_e} \right) \left(\frac{\theta_e}{r_e} \right) - \left(\frac{\delta_e^*}{r_e} \right) \right] \right\}_{\substack{\text{TDK} \\ \epsilon}} (\epsilon' - \epsilon) \\ & - \frac{\partial}{\partial \epsilon} \left[\sum_{\substack{\text{TDK} \\ (\text{O/F})_{i,vap}^* \\ \text{HL} \\ \epsilon}} I_{sp_i} \left(\frac{\dot{m}_{i,vap}^*}{\dot{m}_t} \right) \right] (\epsilon' - \epsilon) \quad (8) \end{aligned}$$

The next step is to develop simplified approximations and methods of evaluation for both the first and second terms of Eq. (7). The evaluation of the boundary-layer loss, $\Delta_2 I_{sp_{BL}}$, is treated separately in Appendix A.

As a first step, Eq. (7) can be written as⁹

$$I_{sp_{pred}} = \eta_{I_{sp_{HL}}} \eta_{I_{sp_{2D}}} \sum_{\substack{ODK \\ (O/F)_{i,vap}^* \\ \epsilon}} I_{sp_i} \left(\frac{\dot{m}_{i,vap}^*}{\dot{m}_t} \right) - \Delta_2 I_{sp_{BL}} \quad (9)$$

where

$$\eta_{I_{sp_{HL}}} = \left[\frac{\sum_{\substack{TDK \\ (O/F)_{i,vap}^* \\ HL}} I_{sp_i} \left(\frac{\dot{m}_{i,vap}^*}{\dot{m}_t} \right)}{\sum_{\substack{TDK \\ (O/F)_{i,vap}^*}} I_{sp_i} \left(\frac{\dot{m}_{i,vap}^*}{\dot{m}_t} \right)} \right]_{\substack{H_{inj} \\ \epsilon \\ \text{size} \\ \text{shape}}} = \left[\frac{I_{sp} (H_{inj} - \dot{Q}/\dot{m}_t)}{I_{sp_{H_{inj}}}} \right]_{\substack{\epsilon \\ ODE \\ (O/F)_{avg}}} \approx \left[1 - \left(\frac{1}{I_{sp}} \frac{\Delta I_{sp}}{\Delta H} \right) (\Delta H_{HL}) \right] \quad (10)$$

⁹ A somewhat similar development to that following, but using subtractive efficiency increments, is described in Ref. 2.

and

$$\eta_{I_{sp} 2D} = \frac{\left[\begin{array}{c} \sum I_{sp_i} \\ \text{TDK} \\ (\text{O/F})_{i, \text{vap}}^* \end{array} \right] \left(\frac{\dot{m}_{i, \text{vap}}^*}{\dot{m}_t} \right)}{\left[\begin{array}{c} \sum I_{sp_i} \\ \text{ODK} \\ (\text{O/F})_{i, \text{vap}}^* \end{array} \right] \left(\frac{\dot{m}_{i, \text{vap}}^*}{\dot{m}_t} \right)} \approx \left[\frac{I_{sp} 2D}{I_{sp} 1D} \right]_{H_{inj}} \quad (11)$$

ϵ
 size
 shape

The chamber injection-end heat loss factor

$$\eta_{I_{sp} HL}$$

accounts for the convective heat lost to the system from the region upstream of the starting point for the boundary layer (injector faceplate and a portion of the chamber wall) and for radiation loss throughout the chamber; this is the heat lost in addition to that accounted for by the boundary-layer calculations. This factor is less than unity only for that portion of the heat which is lost to the system or transferred to a regenerative coolant so that the measured injection enthalpy is increased; there is no net performance loss when the heat is picked up internally by the propellant (as in an injector manifold and faceplate) and returned to the combustion region. The treatment of the various heat losses as they affect performance is shown in Fig. 4. The heat loss is converted to an enthalpy loss by dividing by the total propellant flow rate. The sensitivity of the specific impulse to enthalpy change can be determined by computing ODE performance using perturbed values of the standard propellant enthalpies; the results can be plotted in the form of $[(1/I_{sp})(\Delta I_{sp}/\Delta H)]$ versus propellant mixture ratio for various nozzle exit area ratios, as shown in Appendix B, Fig. B-4. This factor can then be used, as shown by Eq. (10), to calculate the corresponding specific impulse correction factor.

The two-dimensional nature of the nozzle flow affects both the pressure at the nozzle exit and the net axial component of the exit momentum. It also affects the mass flow rate through the nozzle throat and the distribution of pressure and pressure-dependent properties in the boundary-layer flow in the nozzle. The effect of two-dimensional flow on specific impulse is given by the factor

$$\eta_{I_{sp}}^{2D}$$

This factor is given for several common nozzle configurations in Ref. 1, and results for conical nozzles are reproduced here as Figs. 5, 6, and 7.

Equation (9) represents the first useful stage in the simplification of the performance calculation procedure; it substitutes the ODK computer program for the more complicated and expensive-to-use TDK computer program, by introducing the factor

$$\eta_{I_{sp}}^{2D}$$

and it accounts for the heat loss in the chamber upstream of the boundary-layer attachment point by means of the factor

$$\eta_{I_{sp}}^{HL}$$

These factors can be completely or partially precomputed, usually using simplified approximations to the formal defining equations (Eqs. 10 and 11), and charts can be prepared for use in the simplified performance prediction procedures.

A further simplification of Eq. (9) is obtained by replacing each calculated ODK_i stream-tube performance with an ODE_i performance multiplied by an appropriate kinetic efficiency factor. Thus,

$$I_{sp_{pred}} = \eta_{I_{sp_{HL}}} \eta_{I_{sp_{2D}}} \sum \eta_{I_{sp_{i_{kin}}}} I_{sp_{i_{ODE}}} \left(\frac{\dot{m}_{i,vap}^*}{\dot{m}_t} \right) - \Delta_2 I_{sp_{BL}} \quad (12)$$

ϵ
 $(O/F)_{i,vap}^*$

where

$$\eta_{I_{sp_{i_{kin}}}} = \left[\frac{I_{sp_{i_{ODK}}}}{I_{sp_{i_{ODE}}}} \right]_{\epsilon, \text{size, shape}} (O/F)_{i,vap}^* \quad (13)$$

In Eq. (12) each of the factors inside the summation sign is evaluated for the evaporated mixture ratio of the particular stream tube, and for the geometrical nozzle area ratio.

The kinetic loss factor

$$\eta_{I_{sp_{i_{kin}}}}$$

arises from the fact that the combustion gas composition cannot change fast enough to follow the equilibrium composition corresponding to the changes in pressure and temperature as the gases expand through the nozzle. This factor must be calculated for a specific propellant, operating conditions, and thrust chamber size and shape, as shown by Eq. (13), using the ODE and ODK computer programs. For a given propellant and nozzle, values of

$$\eta_{I_{sp, kin}}$$

can be precomputed, as shown in Appendix B, Fig. B-3.

Equation (12) represents the preferred simplified performance prediction procedure. It is the method that should be used if the stream-tube evaporated mass fraction and mixture-ratio distribution is given (as from a DER computer program calculation), or is provided from some other source, or can be reasonably estimated.

The final stage in the development of a simplified performance equation from Eq. (7) is to express the performance in terms of a series of efficiency factors, each of which represents the effect (mass-averaged over all stream tubes) of a specified physical loss process on the overall performance, with the performance referenced to the ODE vacuum specific impulse at the overall average mixture ratio. To do this it is necessary to introduce two new efficiency factors which account for the effects of propellant vaporization and of mixture-ratio distribution on the overall performance; the product of these two efficiencies is defined as the energy-release efficiency.

The final form of the simplified performance equation then becomes

$$I_{sp, pred} = \left[\eta_{I_{sp, HL}} \eta_{I_{sp, 2D}} \eta_{I_{sp, kin}} \eta_{I_{sp, vap}} \eta_{I_{sp, (O/F)dist}} \right] I_{sp, CDE} \epsilon \left(\frac{O}{F} \right)_{avg} - \Delta I_{sp, BL} \quad (14)$$

The vaporization loss is defined by

$$\eta_{I_{sp} \text{ vap}} = \left[\frac{\sum_{\text{ODE}} I_{sp} \left(\frac{\dot{m}_{i, \text{vap}}^*}{\dot{m}_t} \right)}{(O/F)_{i, \text{vap}}^*} \right]_{H_{inj}} \quad (18)$$

and the mixture-ratio distribution, or stream-tube loss, is defined by

$$\eta_{I_{sp} (O/F) \text{ dist}} = \left[\frac{\sum_{\text{ODE}} I_{sp_i} \left(\frac{\dot{m}_{i, \text{inj}}}{\dot{m}_t} \right)}{I_{sp} \text{ ODE } (O/F)_{\text{avg}}} \right]_{H_{inj}} \quad (19)$$

The two above-defined losses, which concern the uniformity of mixing and the completeness of droplet evaporation, are closely related and can be grouped together as the energy-release loss. Thus,

$$\eta_{I_{sp} \text{ ER}} = \left[\eta_{I_{sp} \text{ vap}} \eta_{I_{sp} (O/F) \text{ dist}} \right] = \left[\frac{\sum_{\text{ODE}} I_{sp_i} \left(\frac{\dot{m}_{i, \text{vap}}^*}{\dot{m}_t} \right)}{I_{sp} \text{ ODE } (O/F)_{\text{avg}}} \right]_{H_{inj}} \quad (20)$$

The vaporization loss factor (Eq. 18) accounts for the fact that only that fraction of the injected liquid which evaporates can react and release its

chemical energy to produce thrust. It also accounts for the fact that nonuniform droplet evaporation can cause vaporized mixture-ratio distributions (at the nozzle throat) which differ from the injected mixture-ratio distributions.

The vaporized mass and mixture-ratio distribution needed to evaluate

$$\eta_{I_{sp}}^{vap}$$

are obtained from the DER computer program calculation, which in turn requires as input a complete description of the injected mass, mixture-ratio, and droplet-size distributions.

The primary mixture-ratio distribution loss (Eq. 19) arises from non-uniform injected mixture-ratio distribution. With the usual concave-downward variation of specific impulse with propellant mixture ratio, the mass-averaged performance of a distributed mixture-ratio flow is typically less than the performance which would be achieved with the entire flow at its average mixture ratio.

The boundary-layer loss efficiency factor

$$\Delta \eta_{I_{sp}}^{BL}$$

used in Eqs. (15) and (16) is defined as

$$\Delta \eta_{I_{sp}}^{BL} = \frac{\Delta_2 I_{sp}^{BL}}{I_{sp}^{ODE} (O/F)_{avg}} \quad (21)$$

where the specific impulse loss

$$\Delta_2 I_{sp}^{BL}$$

is defined by Eq. (8). The evaluation of the boundary-layer loss is discussed in more detail in Appendix A.

The reference ideal performance

$$I_{sp}^{ODE} \text{ (O/F)avg}$$

used in Eqs. (13) through (21) is evaluated for the specified test conditions of propellant composition (including impurities), injector inlet enthalpy, overall mixture ratio, chamber pressure, and nozzle exit-area ratio.

The ODE (one-dimensional isentropic equilibrium) performance is often available from calculations made for the propellants at standard tabulated initial enthalpy values. Performance at actual inlet enthalpy conditions can be obtained by correcting this standard enthalpy performance, using the specific impulse-enthalpy influence factor developed to correct for heat loss from the combustion chamber walls (cf Eq. 10 and Appendix B, Fig. B-4).

If the efficiency factors in Eq. (15) are evaluated according to the primary defining equations (Eqs. 17 through 23), Eq. (15) will yield the same predicted performance that would be given by Eq. (7) or Eq. (12). However, it must be recognized that, when the flow mixture-ratio distribution spans a region in which the performance (or an efficiency factor) is nonlinear with mixture ratio, apparent, but compensating, distortions will be introduced into related terms of Eq. (15). This is caused by using a reference specific impulse which corresponds to the average mixture ratio of a striated flow.

Thus, if two stream tubes have mixture ratios below and above the mixture ratio for maximum performance, the reference specific impulse will be higher than the actual specific impulse of either stream tube, and the specific impulse efficiency for mixture-ratio distribution will have to be correspondingly low. However, if the stream-tube mixture ratios spanned a region in which the performance was nearly linear with mixture ratio, the specific impulse at the average mixture would be a "real" value, and the specific impulse efficiency for mixture-ratio distribution would be near 100%.

Similarly, an error can be introduced by choosing a specific impulse efficiency for kinetic effects at the average mixture ratio, rather than using

a mass-averaged value for the actual stream mixture ratios. Other distortions could be caused by the effect of vaporization efficiency in changing effective stream-tube mixture ratios.

Additional distortions in the relative values of the loss efficiency factors, but no net error in the calculated performance, can result from the fact that there are interactions between the loss processes which cannot be correctly assigned when the losses are individually defined, as they must be for the simplified procedures developed herein. These effects cancel out internally when the efficiencies are defined according to the primary definitions given here. However, errors can be introduced when the approximate expressions for evaluating some of the loss efficiencies are used; probably the most important interaction involves energy release (vaporization) and kinetics.

The above examples serve to indicate the necessity for care in using the form of the performance prediction equation given by Eq. (15). It is necessary to select values of specific impulse efficiency for kinetics, vaporization, and mixture-ratio distribution effects which correspond to the real stream-tube mass and mixture-ratio and vaporization distributions, or at least to reasonable estimates of these distributions. It should also be kept in mind that, because of the above-mentioned distortions, maximum predicted performance may not correspond to maximum overall specific impulse efficiency. Thus, when two rocket motor systems are being compared, comparison should be on the basis of predicted specific impulse, rather than on overall efficiency.

The above considerations emphasize again that simplified performance prediction by the procedure of Eq. (12) is preferable to that based on Eq. (15), even if it requires estimation or assumption of reasonable mass and mixture-ratio distribution and component vaporization efficiencies.

Equation (15) can be used to make initial estimates of the performance of proposed thrust chambers, or to make parametric design studies around a given configuration. The two-dimensional-flow loss efficiency can be determined from existing design charts. The kinetic, boundary-layer, and upstream chamber heat-loss efficiency terms can be calculated by using the ODK, ODE, and TBL computer programs or charts prepared from these programs. The energy-release efficiency can be calculated from postulated

injection conditions, using the DER computer program and Eq. (14). As a last resort, some or all of these quantities can be estimated on the basis of previous experience.

If it is known that a given propellant system and a range of thrust chamber configurations are to be subjected to thorough analysis, it is worthwhile to use the ODE, ODK, TDE or TDK, and boundary layer computer programs early to investigate a broad parametric range of operating conditions. If feasible, the energy-release efficiency can be precalculated in the same way, using the DER and ODE computer programs. The results of these calculations can be used to develop a set of "influence coefficients," which become the basis of a procedure for correcting design condition performance predictions to obtain predicted performance at actual test conditions or for slightly modified design conditions.¹⁰

The results of a typical set of parametric calculations for the fluorine-hydrazine propellant in a given thrust chamber configuration are presented in Appendix B.

Table 3 of this report summarizes the derivation of the simplified performance prediction equation and the definitions of the specific impulse loss process efficiency factors developed here.

VI. CORRELATION OF EXPERIMENTALLY MEASURED AND PREDICTED VACUUM SPECIFIC IMPULSE

The measured and predicted vacuum specific impulses can be compared to confirm or infer the magnitudes of the individual losses. The losses can then be evaluated and a judgment made as to whether they are individually reasonable and acceptable, or whether thrust chamber or injector design changes should be made in an attempt to decrease the magnitude of those

¹⁰ These influence coefficients are sometimes used inversely to "correct" experimental data to a common reference condition. Such a procedure violates the premise of this report that experiment and analysis should be kept completely separate and independent right up to the point of comparison. However, it is convenient for removing secondary effects from a mass of experimental data so that primary effects can be more clearly recognized, and for facilitating comparison with predicted performance calculated at a "design" reference condition.

losses which are susceptible to control. Some losses, such as the two-dimensional divergence loss, the kinetic loss, and often the boundary-layer loss, are not very susceptible to the control. On the other hand, the energy-release losses (mixture-ratio distribution and vaporization) can be controlled, though usually at the expense of some other deliberately designed-for characteristic, such as low heat flux, chamber wall compatibility, low injector pressure drop, or small combustion chamber size.

If complete operating condition data are available, and it has been possible to use the DER, TDK, ODK, ODE, and boundary layer computer programs to predict all of the loss components, then performance correlation consists of demonstrating that

$$\frac{I_{sp \text{ vac exp}}}{I_{sp \text{ vac pred}}} = \frac{\eta_{I \text{ TC exp}}}{\eta_{I \text{ TC pred}}} = 1 \pm \Delta_{cor} \quad (22)$$

where Δ_{cor} is a correlation parameter defining an acceptable limit of error, based on the uncertainty involved in arriving at the two values of specific impulse; a value of $\Delta_{cor} = 0.01$ or better is suggested as a goal, though higher values may have to be accepted at times.¹¹

If Eq. (22) is not satisfied at the first attempt, agreement within a reasonable limit of error can usually be obtained by recalculation after a careful examination for possible errors in experimental data, input information, and calculation procedures. Correlation in this manner is accepted as confirming that the magnitudes of the separate loss effects shown in Eq. (12) or (15) have been correctly predicted.

¹¹ A more refined statistical approach to the correlation of measured and predicted performance which considers the uncertainty of each quantity will be given in the "JANNAF Performance Data Analysis Manual" being prepared by Rocketdyne under Contract NAS8-28603. The basis for this approach is contained in Statistics, by W. L. Hays, published by Holt, Reinhardt, & Winston, 1963.

The same procedure is followed if some of the loss components have been determined from charts or even estimated on the basis of previous experience. The result in either case is a quantification of losses and corresponding efficiencies which can be used as a basis for evaluation of the thrust chamber design and performance.

Figure 1 shows graphically the above correlation process and the subsequent procedure for evaluating the performance and the losses to determine whether they are acceptable, or whether additional design and development work is needed. At a lower level of sophistication, the injection mixture-ratio and droplet-size distribution input data may not be known, so the DER computer program cannot be used to determine the energy-release efficiency components. In this case, the lumped energy-release losses can be "backed out" of the data (at a reduced confidence level of accuracy, because there is no overall check on the consistency of the results) by the following approximate formula, derived from Eqs. (16), (20), and (22), with the assumption that $\Delta_{cor} = 0$:

$$\eta_{I_{sp}}^{ER} \approx \left[\frac{\eta_{I_{sp}}^{TC} + \Delta\eta_{I_{sp}}^{BL}}{\eta_{I_{sp}}^{exp} \eta_{I_{sp}}^{pred}} \right] \quad (23)$$

$$\left(\eta_{I_{sp}}^{2D} \eta_{I_{sp}}^{kin} \eta_{I_{sp}}^{HL} \right)_{pred}$$

In the above expression, it is presumed that the component loss efficiencies, other than

$$\eta_{I_{sp}}^{ER}$$

can be calculated from the available data, and that actual performance has been measured.

This procedure enables values to be assigned to all of the losses, so that the evaluation process shown in Fig. 1 can be completed. An example of a correlation and evaluation of test data obtained using the fluorine-hydrazine propellant in a given thrust chamber is presented in Appendix C.

VII. PERFORMANCE PREDICTION FOR RELATED THRUST CHAMBER CONFIGURATIONS

The individual loss components determined by correlating the test data obtained with a given thrust chamber can be used as the basis for predicting the performance of related thrust chamber configurations, using the same basic performance prediction and correlation methodology and equations.

Related thrust chamber configurations may range from variations in propellant inlet temperature or changes in chamber wall cooling method and temperature to the addition of a high-area-ratio nozzle extension to a low-area-ratio test motor. Depending on the differences between the modified thrust chamber and/or extrapolated operating conditions, it may be possible to retain a few of the correlated performance efficiency factors without change. The other performance efficiency factors, and perhaps the reference ODE performance, must be adjusted or recalculated according to the defining equations. Then the modified or extrapolated performance is calculated from Eq. (12) or (15).

It will be found that almost every case of performance extrapolation becomes a new problem in performance prediction, requiring recalculation of the reference ODE performance and adjustment of most of the efficiency factors. The recalculation task can be simplified if a sufficiently wide parametric range of calculations is made initially for the propellant system under consideration, as described previously and shown in Appendix B. Appendix C illustrates the use of the calculated factors of Appendix B in correlating test data and in "extrapolating" to performance at a different nozzle exit-area ratio.

VIII. EXPERIMENTAL DETERMINATION OF CHARACTERISTIC VELOCITY

The objective of this and the following sections of this report is to define the performance parameter, characteristic velocity c^* , and to develop a procedure for predicting and correlating this parameter which is consistent with the JANNAF thrust chamber model and specific impulse prediction methodology.

The characteristic velocity is a mass-flow performance parameter. It is related to the energy release in the combustion chamber up to the nozzle throat, where the mass flow is determined. The definition of the experimentally measured c^* is¹²

$$c_{\text{exp}}^* = \frac{\bar{p}_0^* A_t}{\dot{m}} \quad (24)$$

¹²As defined, c^* has units of $[F t/M]$. Since force is a derived unit which is defined in terms of the basic $[L, M, t]$ units, c^* , as well as I_{sp} , can be expressed in the alternate, but equivalent, $[L/t]$ units. This is accomplished by multiplying by the unity unit conversion ratio corresponding to the measurement system being used. In the SI system this unity ratio is

$$1 \equiv \left[\frac{1.0 \text{ kg}\cdot\text{m}}{\text{N}\cdot\text{sec}^2} \right]$$

In the English technical system of units, this unity ratio is

$$1 \equiv \left[\frac{32.174 \text{ lbm}\cdot\text{ft}}{\text{lbf}\cdot\text{sec}^2} \right]$$

Equivalent quantities of specific impulse and characteristic velocity in both the SI and the English technical systems are summarized in the following "conversion box":

$1 \left[\frac{\text{lbf}\cdot\text{sec}}{\text{lbm}} \right] \equiv 32.174 \left[\frac{\text{ft}}{\text{sec}} \right]$
$9.806 \left[\frac{\text{N}\cdot\text{sec}}{\text{kg}} \right] \equiv 9.806 \left[\frac{\text{m}}{\text{sec}} \right]$

where

\bar{p}_0^* is a mean effective stagnation pressure at the nozzle throat. It is determined from the relation $\bar{p}_0^* = p_{s_x} (\bar{p}_0^*/p_{s_x})$.

$\left(\frac{\bar{p}_0^*}{p_{s_x}}\right)$ is estimated from the well-known analysis for combustion in a cylindrical combustion chamber, depending on the tap location (see Fig. 8).

A_t is the nozzle throat area during thrust chamber operation. It is usually determined by correcting the "cold" throat area for effects due to pressure, thermal expansion and thermal stress, erosion, etc.

p_{s_x} is a static pressure measured at the wall of the combustion chamber nozzle at the longitudinal station x .

At this point, it is convenient to define an overall thrust chamber characteristic velocity efficiency:

$$\eta_{c_{TC}^*}^{\text{exp}} = \frac{c_{\text{exp}}^*}{c_{\text{ODE}}^* (O/F)_{\text{avg}}} \quad (25)$$

Here

$$c_{\text{ODE}}^* (O/F)_{\text{avg}}$$

is the ideal characteristic velocity that would be attained in the absence of all of the real thrust chamber internal loss processes. It is calculated using the ODE computer program for the actual thrust-chamber-test injector-inlet propellant composition and enthalpy. Note that for a regeneratively cooled thrust chamber, the injector-inlet propellant enthalpy must include the heat transferred to the propellant from the chamber, and is not the propellant enthalpy at the engine inlet.

It is desirable that the experimental value of a performance parameter be derived directly from the measured test data, without involving any

analytically based corrections whatsoever. Though this criterion is satisfied by the definition of the experimental vacuum specific impulse, it cannot be completely satisfied in the definition of experimental characteristic velocity because the basic definition of c^* logically involves the stagnation pressure at the nozzle throat, where the mass flow is determined. Determination of the throat stagnation pressure to be used in the calculation of c^* is complicated by the facts that (1) with multi-stream-tube flow, each stream tube has a different stagnation pressure, so that some sort of a mean value must be defined and used; and (2) it is not possible to measure directly the stagnation pressure of the flow in the throat of a rocket nozzle.

The only pressure relevant to the stagnation pressure that can be measured is the static pressure p_{s_x} at some longitudinal station x on the wall of the thrust chamber. An analytically based correlation factor, (\bar{p}_0^*/p_{s_x}) , is then used to obtain a value for the mean effective stagnation pressure at the nozzle throat.¹³

For an ideal rocket engine with uniform perfect gas flow and a cylindrical combustion chamber, the factor (\bar{p}_0^*/p_{s_x}) is well defined and presented in the literature (see Fig. 8). This is the factor commonly used in computing characteristic velocity from the experimental data for all types of rocket motors.

When the combustion chamber is not cylindrical and/or there is multi-stream-tube flow, the ideal rocket engine factor does not apply. However, the DER computer program can be used for these cases to analyze the flow and to determine the static pressure-stagnation pressure relationships as well as the droplet evaporation and combustion efficiency.¹⁴ The results of a recent application of DER to determine the static pressure-stagnation

¹³Static pressure measurements made in the injection region of the chamber may be in error by several percent due to local aspiration effects. A mid-chamber or nozzle-entrance static pressure measurement is generally acceptable.

¹⁴The availability of the DER computer program opens up the possibility of defining and using a new mass-flow parameter based on a measured static pressure. The DER computer program would enable prediction of the static pressure at the location of the pressure measurement, and, thus, prediction of the analytical counterpart of this new parameter. However, this parameter would lack the generality of the present c^* .

pressure relationship for multi-stream-tube flow with droplet-evaporation-limited combustion in a noncylindrical chamber are described in Ref. 4.

An additional slight departure from the criterion of using only direct measurements in the calculation of experimental performance parameters occurs in the determination of the throat area to be used in calculating the characteristic velocity. Since it is not feasible to measure the throat area during motor operation, it is customary to measure this area under "cold" pre-test conditions and apply appropriate corrections for thermal expansion and stress, pressure, erosion, etc. These corrections are generally quite small.

As a consequence of the considerations discussed above, it must be accepted that the characteristic velocity c_{exp}^* has an inherent uncertainty of 2 to 3%. This arises largely from the uncertainty in inferring \bar{p}_0^* from a measured static wall pressure p_{sx} , especially when there is multi-stream-tube flow through the nozzle, or when the combustion occurs in other than a cylindrical chamber. Despite this uncertainty in absolute level, c_{exp}^* can be compared with c_{pred}^* to give a useful first look at the magnitude of the losses involved in the thrust chamber combustion process.

IX. SIMPLIFIED FORM FOR ANALYTICAL PREDICTION OF CHARACTERISTIC VELOCITY

A close analytical approximation, following the JANNAF thrust chamber combustion and loss model, to the experimental characteristic velocity defined in the preceding section is

$$c_{pred}^* = \frac{\bar{p}_0^* A_t}{\dot{m}_t} = \frac{\sum_{ODK} c_i^* \left(\frac{\dot{m}_{i,vap}}{\dot{m}_t} \right) (O/F)_{i,vap}^*}{HL} \frac{1}{C_D \left(1 - \frac{2\delta_t^*}{r_t} \right)} \quad (26)$$

where $c_{i,vap}^*$, $\dot{m}_{i,vap}^*$, and $(O/F)_{i,vap}^*$ correspond to the local stream-tube vaporized mass and mixture ratio at the throat.

Expression (26) is an adequate approximation to the overall mass-flow parameter as long as the liquid droplet fraction is a small part of the total mass flow. It is derived by summing the one-dimensional thermodynamic stream-tube throat areas and equating them to the total effective throat area, derived by correcting the geometrical throat area for boundary-layer and two-dimensional flow effects. It is assumed that the individual stream-tube stagnation pressures can be replaced by a single mean stream-tube stagnation pressure, and that multi-stream-tube-flow sonic-point-displacement effects on the effective throat area are negligible.

Expression (26) for predicted characteristic velocity can be recast as

$$\begin{aligned}
 c_{\text{pred}}^* &= c_{\text{(O/F)avg}}^* \text{ODE} \left[\eta_{c_{2D}}^* \eta_{c_{\text{kin}}}^* \eta_{c_{\text{vap}}}^* \eta_{c_{\text{(O/F)dist}}}^* \eta_{c_{\text{HL}}}^* \eta_{c_{\text{BL}}}^* \right] \\
 &= c_{\text{(O/F)avg}}^* \text{ODE} \eta_{c_{\text{TC pred}}}^*
 \end{aligned}
 \tag{27}$$

The terms in the above expressions are defined and evaluated as follows, where each factor η corresponds to a specific loss:

$$(1) \quad c_{\text{(O/F)avg}}^* \text{ODE}$$

is evaluated at the specified test conditions of chamber pressure, overall mixture ratio, propellant composition (including impurities), and inlet enthalpy. For a regeneratively cooled motor, the inlet enthalpy must include all of the heat transferred from the thrust chamber to the propellant.

- (2) The two-dimensional nature of the flow results in a curvature of the sonic surface and a net decrease in the effective one-dimensional flow area. This in turn results in a loss factor

$$\eta_{c_{2D}}^* = \frac{1}{C_{D_{2D}}} \tag{28}$$

Values of this factor are given as a function of the throat radius ratio in the summary chart prepared by Back and Cuffel (Figs. 9 and 10 and Ref. 3).

- (3) The kinetic loss arises from the fact that the combustion gas equilibrium cannot change fast enough to follow the changes in pressure and temperature as the gases expand through the nozzle. This effect is rarely important upstream of the nozzle throat, and thus has little effect on the characteristic velocity. The corresponding loss factor is

$$\eta_{c^* \text{ kin}} = \frac{\sum_i c_i^* \left(\frac{\dot{m}_{i, \text{ vap}}^*}{\dot{m}_t} \right)}{\sum_i c_i^* \left(\frac{\dot{m}_{i, \text{ vap}}^*}{\dot{m}_t} \right)} = \left[\frac{c_{\text{ODK}}^*}{(O/F)_{\text{avg}}^*} \right]_{H_{\text{inj}} \text{ size shape}} \quad (29)$$

This factor must be calculated for the specific propellant, operating conditions, and thrust chamber size and shape, as defined by Eq. (25), using the ODE and ODK computer programs.

- (4) The vaporization loss factor accounts for the fact that the fraction of the propellant which has evaporated and reacted occupies most of the cross-sectional area of the nozzle throat. It also accounts for the fact that nonuniform droplet evaporation can cause vaporized mixture-ratio distributions (at the nozzle throat) which differ from the injected mixture-ratio distributions. This factor is defined as

$$\eta_{c^* \text{ vap}} = \left[\frac{\sum_i c_i^* \left(\frac{\dot{m}_{i, \text{ vap}}^*}{\dot{m}_t} \right)}{\sum_i c_i^* \left(\frac{\dot{m}_{i, \text{ inj}}}{\dot{m}_t} \right)} \right]_{H_{\text{inj}}} \quad (30)$$

The vaporized mass and mixture-ratio distributions needed to calculate $\eta_{c_{\text{vap}}}^*$ are obtained from the DER computer program calculation, which in turn requires as input a complete description of the injected-mass, mixture-ratio, and droplet-size distributions.

- (5) The primary mixture-ratio loss arises from nonuniform injected mixture-ratio distribution. With the usual concave-downward variation of characteristic velocity with mixture ratio, the mass-averaged performance of a distributed mixture-ratio flow is less than the performance that would be achieved with the entire flow at its average mixture ratio. The factor accounting for this loss is

$$\eta_{c_{\text{(O/F)dist}}}^* = \frac{\sum_{\text{ODE}} c_i^* \left(\frac{\dot{m}_{i, \text{inj}}}{\dot{m}_t} \right)}{c_{\text{(O/F)avg}}^* \text{ODE}} \Bigg]_{H_{\text{inj}}} \quad (31)$$

- (6) The chamber injection-end heat-loss factor is defined as

$$\eta_{c_{\text{HL}}}^* = \frac{\sum_{\text{ODK}} c_i^* \left(\frac{\dot{m}_{i, \text{vap}}^*}{\dot{m}_t} \right)}{\sum_{\text{ODK}} c_i^* \left(\frac{\dot{m}_{i, \text{vap}}^*}{\dot{m}_t} \right)} \approx \left[\frac{c_{H_{\text{inj}}}^* - (\dot{O}/\dot{m}_t)}{c_{H_{\text{inj}}}^*} \right]_{\text{ODE}} \text{(O/F)avg}$$

$$\approx \left[1 - \left(\frac{1}{c^*} \frac{\Delta c^*}{\Delta H} \right) \Delta H_{\text{HL}} \right] \quad (32)$$

This factor accounts for the convective heat lost to the system from the region (injector faceplate and a portion of the chamber

wall) upstream of the starting point for the boundary layer, and for radiation loss throughout the chamber; this is the heat lost in addition to that accounted for by the boundary-layer calculations. This factor is less than unity only for the heat which is lost to the system or transferred to a regenerative coolant so that the measured injection enthalpy is increased; there is no net performance loss when the heat is picked up internally by the propellant (as in an injector faceplate and manifold) and returned to the combustion region (see Fig. 4).

- (7) The boundary-layer performance loss arises from friction and from cooling of the combustion products near the wall. The effect is usually to reduce the effective inviscid-flow area of the nozzle throat. The corresponding performance loss factor is

$$\eta_{c_{BL}}^* = \frac{1}{\left(1 - \frac{2\delta_t^*}{r_t}\right)} \quad (33)$$

The boundary-layer displacement thickness δ_t^* is obtained from a boundary-layer program such as TBL, using TDK property output.

The boundary-layer displacement thickness at the throat can become negative if the wall is highly cooled. Because of the accelerating flow through the throat, the boundary layer in this region is usually very thin, so that $\eta_{c_{BL}}^*$ is usually very close to unity.

Two of the above-defined losses, related to the uniformity of the mixing and the completeness of the evaporation, can be grouped together as an energy-release loss. Thus,

$$\eta_{c_{ER}}^* = \left[\eta_{c_{vap}}^* \eta_{c_{(O/F)dist}}^* \right] = \frac{\left[\sum_i c_i^* \left(\frac{\dot{m}_{i,vap}^*}{\dot{m}_t} \right) \right]_{ODE} (O/F)_{i,vap}}{c_{ODE}^* (O/F)_{avg}} H_{inj} \quad (34)$$

It is often convenient to consider η_{c^*ER} as a whole, since its individual components are related and interacting.

The derivation and definition of the characteristic velocity efficiency factors are summarized in Table 4.

X. CORRELATION OF EXPERIMENTALLY MEASURED AND PREDICTED CHARACTERISTIC VELOCITY AND COMPARISON WITH SPECIFIC IMPULSE PARAMETERS

As is the case with specific impulse, the measured and predicted characteristic velocities can be compared to confirm or infer the magnitude of the individual losses. The losses can then be evaluated and a judgment made as to whether they are individually reasonable and acceptable, or whether thrust chamber or injector design changes should be made in an attempt to decrease the magnitude of those losses which are susceptible to control. The two-dimensional flow, kinetic, upstream chamber heat-transfer, and boundary-layer characteristic velocity losses are generally small. This leaves the energy-release losses (vaporization and mixture-ratio distribution) as the major factors in the overall characteristic velocity efficiency; these are also the losses most susceptible to individual control by changes in injector and chamber design. However, the control will often be at the expense of some other deliberately designed-for characteristic, such as low heat flux, chamber wall compatibility, low injector pressure drop, or small combustion-chamber size.

A common application of characteristic velocity correlation is to obtain a first look at the energy-release efficiency, "backing it out" of the experimental data and the more easily estimated losses, according to the equation:¹⁵

$$\eta_{c^*ER} = \eta_{c^*vap} \eta_{c^*(O/F)dist} \approx \frac{\eta_{c^*TC, exp}}{[\eta_{c^*2D} \eta_{c^*kin} \eta_{c^*HL} \eta_{c^*BL}]_{pred}} \quad (35)$$

¹⁵The bracketed term in the denominator of Eq. (35) usually differs only slightly from unity, so that as a rough approximation $\eta_{c^*ER} \approx \eta_{c^*TC, exp}$.

It must be remembered that vacuum specific impulse and the various specific impulse efficiencies are the ultimately important quantities in the design and operation of rocket motors. Characteristic velocity is a different performance parameter from specific impulse, and characteristic velocity efficiencies are not identical to the corresponding specific impulse efficiencies. However, the energy-release components of both the specific impulse efficiency and the characteristic velocity efficiency are related in that they are both ratios of mass-averaged values of their respective quantities over the evaporated mass and mixture-ratio range compared to the value of the quantity at the average injected mixture ratio (see Eqs. 14 and 30). It is clear that

$$\eta_{I_{sp}}^{ER} \quad \text{and} \quad \eta_{c^*}^{ER}$$

will both respond in the same manner to a deficiency in evaporated mass flow, and both will be influenced by the relative curvature of their respective values as functions of mixture ratio in the operating mixture-ratio region. In fact, if I_{sp}^{vac} and c^* were exactly similar functions of mixture ratio, the two energy-release efficiencies would be identical, but this condition is generally not exactly satisfied.

Inspection of the relative curvature of the I_{sp}^{vac} and c^* curves as functions of mixture ratio in the operating mixture-ratio region should give an indication of the relative response of the corresponding energy-release efficiencies to mixture-ratio distribution for a given propellant; it will usually be found that the specific impulse efficiency (at all nozzle area ratios) and the characteristic velocity efficiency are affected about equally by mixture-ratio distribution. Thus,

$$\eta_{c^*}^{ER} \approx \eta_{I_{sp}}^{ER} \approx \eta_{I_{sp}}^{ER}$$

low ϵ high ϵ

The difference between these quantities will usually be small.

The above relationships can be used in estimating

$$\eta_{I_{sp}}^{c_{ER}}$$

from an experimentally determined value of $\eta_{c_{ER}}^*$. This is often a convenient first step in a thrust chamber development or evaluation program, since the necessary testing can be conducted using a low-area-ratio thrust chamber in an ambient pressure environment and on a fixed test stand without thrust measurement. However, the slight extra effort of measuring thrust as well as propellant flow rate and chamber pressure, even in initial phases of testing and with low-exit-area-ratio thrust chambers, is generally worthwhile, as it enables determination of the ultimately needed specific impulse parameters.

In conclusion, it should be stated that while characteristic velocity is a useful performance parameter in its own right (relating mass flow to throat area and chamber pressure), it is not a substitute for specific impulse. Specific impulse data are an essential requirement for thrust chamber development and for performance correlation and prediction, and provision for obtaining the needed test data should be included in any such development program.

Table 1. Thrust chamber performance losses

- | | |
|----|---|
| 1. | Chamber heat loss (upstream of boundary-layer start point) |
| 2. | Two-dimensional flow |
| 3. | Kinetics: rate-limited equilibrium shift during expansion |
| 4. | Vaporization: incomplete liquid droplet evaporation up to nozzle throat |
| 5. | Mixture-ratio distribution at injection |
| 6. | Boundary layer: friction and heat transfer at chamber and nozzle walls |

Table 2. Thrust chamber performance computer programs

- | | | |
|----|---------------|--|
| 1. | ODE | One-dimensional equilibrium combustion and nozzle flow |
| 2. | DER | Distributed energy release: mixture-ratio distribution and droplet evaporation up to nozzle throat |
| 3. | ODK | One-dimensional kinetic multi-zone nozzle flow |
| 4. | TDK | Two-dimensional kinetic multi-zone nozzle flow |
| 5. | TBL | Boundary layer, integral method |
| 6. | MABL
BLIMP | Boundary layer, finite difference method, including mass addition |

Table 4. Development of approximate method for predicting characteristic velocity

$$\begin{aligned}
 (1) \quad c_{\text{exp}}^{\text{O}} &= \frac{\bar{p}_t A_t}{\dot{m}_t} \\
 (2) \quad c_{\text{pred}}^{\text{O}} &= \sum_{\text{ODE}} c_{\text{ODE}}^{\text{O}} \left(\frac{\dot{m}_{1,\text{vap}}}{\dot{m}_t} \right) \frac{1}{C_{D,2D}} \frac{1}{\left(1 - \frac{2\delta_{\text{O}}^{\text{O}}}{r_t} \right)} \\
 &\quad \text{HL} \\
 (3) \quad c_{\text{pred}}^{\text{O}} &= \frac{\sum_{\text{ODE}} c_{\text{ODE}}^{\text{O}} \left(\frac{\dot{m}_{1,\text{vap}}}{\dot{m}_t} \right) \frac{1}{C_{D,2D}} \frac{1}{\left(1 - \frac{2\delta_{\text{O}}^{\text{O}}}{r_t} \right)}}{\sum_{\text{ODE}} c_{\text{ODE}}^{\text{O}} \left(\frac{\dot{m}_{1,\text{vap}}}{\dot{m}_t} \right)} \times \frac{\sum_{\text{ODE}} c_{\text{ODE}}^{\text{O}} \left(\frac{\dot{m}_{1,\text{vap}}}{\dot{m}_t} \right) \frac{1}{C_{D,2D}} \frac{1}{\left(1 - \frac{2\delta_{\text{O}}^{\text{O}}}{r_t} \right)}}{\sum_{\text{ODE}} c_{\text{ODE}}^{\text{O}} \left(\frac{\dot{m}_{1,\text{vap}}}{\dot{m}_t} \right)} \times \frac{1}{C_{D,2D}} \frac{1}{\left(1 - \frac{2\delta_{\text{O}}^{\text{O}}}{r_t} \right)} \\
 &\quad \text{HL} \quad \text{kinetic} \quad \text{vapor} \quad \text{injection} \\
 (4) \quad c_{\text{pred}}^{\text{O}} &= \left[\eta_{\text{HL}} \times \eta_{\text{kinetic}} \times \eta_{\text{vapor}} \times \eta_{\text{injection}} \right] c_{\text{ODE}}^{\text{O}} \left(\frac{\dot{m}_{1,\text{vap}}}{\dot{m}_t} \right) \frac{1}{C_{D,2D}} \frac{1}{\left(1 - \frac{2\delta_{\text{O}}^{\text{O}}}{r_t} \right)} \\
 &\quad \text{HL} \quad \text{kinetic} \quad \text{vapor} \quad \text{injection}
 \end{aligned}$$

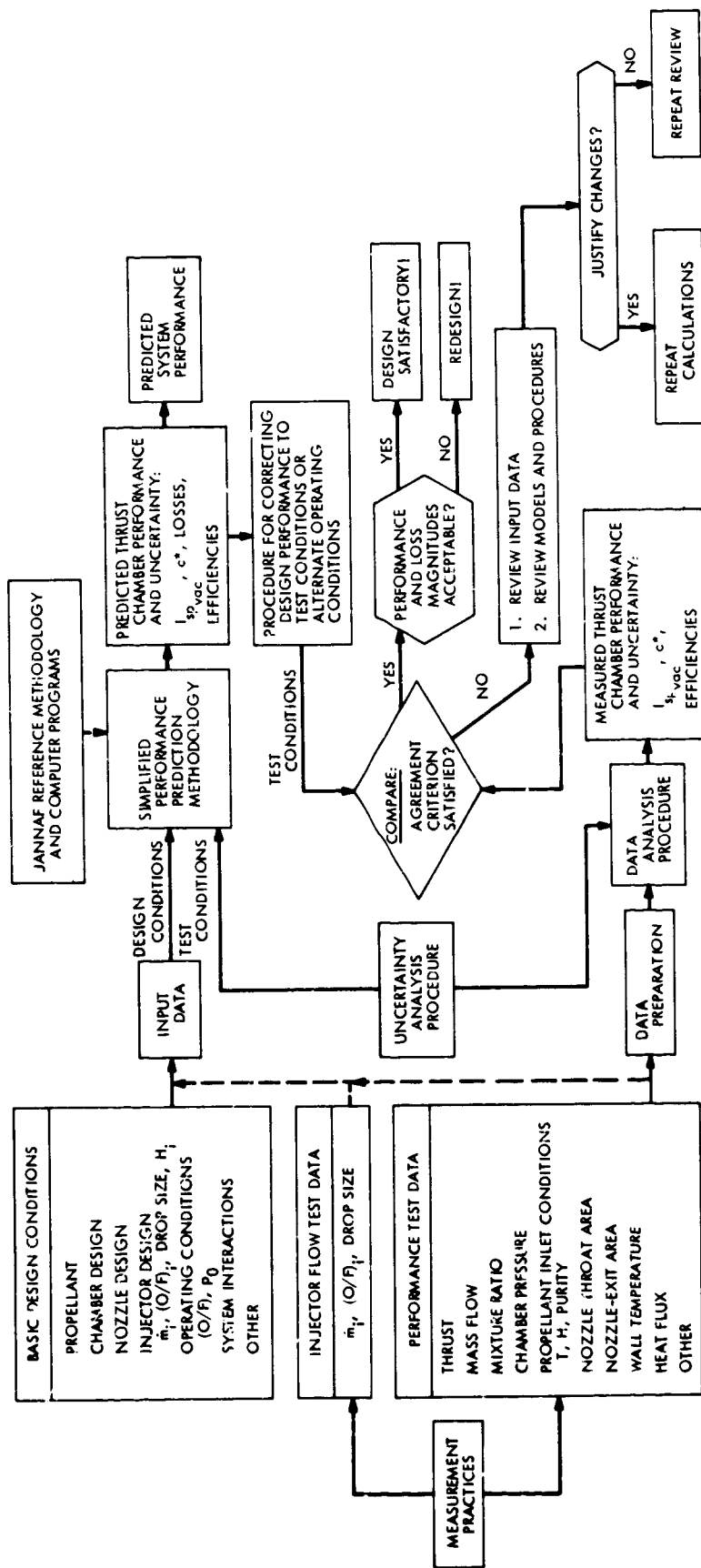


Fig. 1. Simplified performance prediction and correlation procedure chart

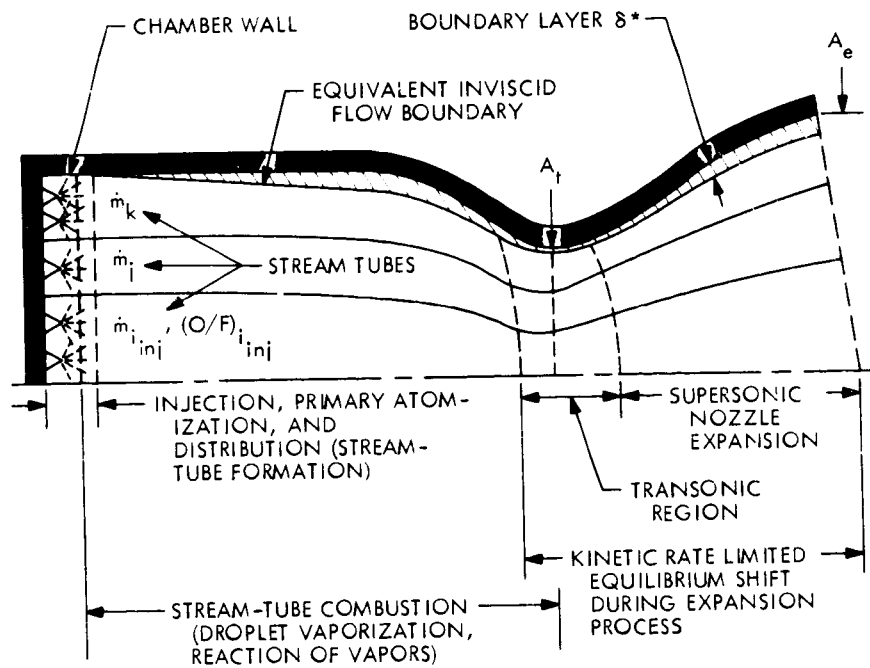


Fig 2. Internal processes in the real rocket thrust chamber

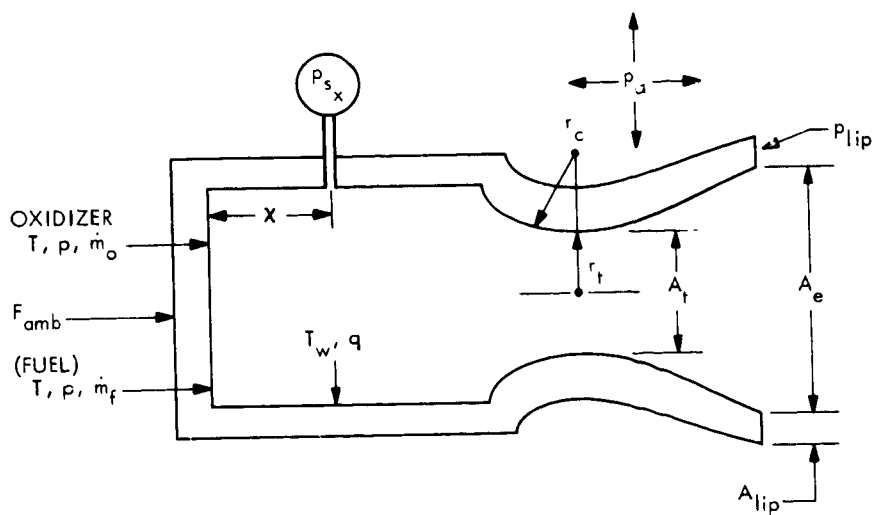
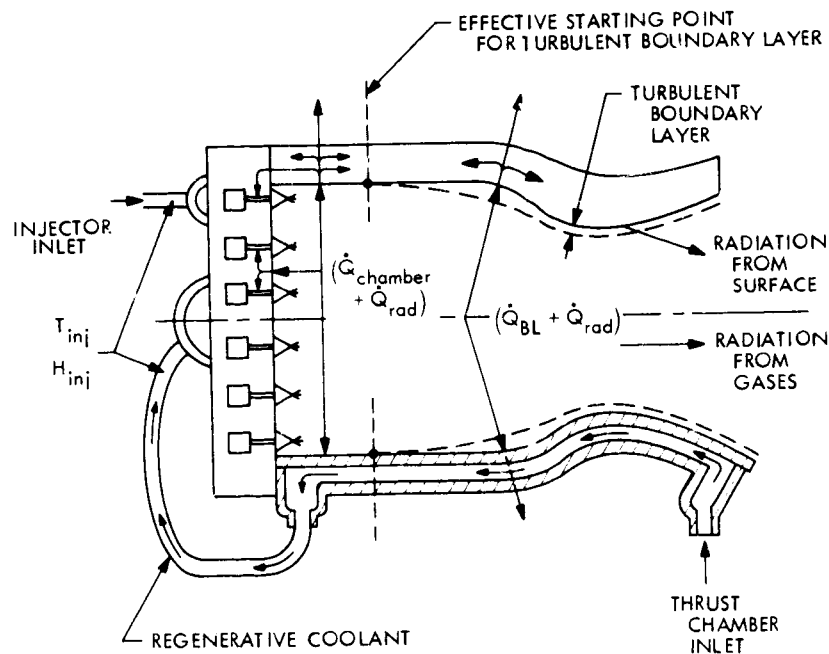


Fig. 3. Experimental data needed for thrust chamber performance and evaluation



HEAT FLOW

EFFECT ON THRUST CHAMBER PERFORMANCE CALCULATION

$(\dot{Q}_{BL} + \dot{Q}_{rad})$ IN TURBULENT BOUNDARY-LAYER REGION.

BOUNDARY LAYER COMPUTER PROGRAM ACCOUNTS FOR EFFECT OF \dot{Q}_{BL} ON PERFORMANCE. SUBTRACT \dot{Q}_{rad}/m_t FROM H_{inj} TO ACCOUNT FOR RADIATION HEAT LOSS. NOTE THAT ANY PART OF THIS HEAT PICKED UP BY REGENERATIVE COOLANT INCREASES H_{inj} AND THE REFERENCE ODE PERFORMANCE LEVEL.

$(\dot{Q}_{chamber} + \dot{Q}_{rad})$ IN REGION UPSTREAM OF TURBULENT BOUNDARY-LAYER ATTACHMENT POINT.

- A. HEAT STORED IN THE WALL, LOST TO THE OUTSIDE, OR PICKED UP BY REGENERATIVE COOLANT IN SUCH A MANNER THAT THE MEASURED H_{inj} IS INCREASED.
- B. HEAT TRANSFERRED TO PROPELLANT AND RE-INTRODUCED INTO THE THRUST CHAMBER INTERNALLY (WITHOUT SHOWING UP AT THE POINT WHERE H_{inj} IS MEASURED).

- A. SUBTRACT ENTHALPY CORRESPONDING TO THIS PORTION OF THE HEAT FLOW FROM THE MEASURED H_{inj} . NOTE THAT ANY PART OF THIS HEAT PICKED UP BY REGENERATIVE COOLANT INCREASES H_{inj} AND THE REFERENCE ODE PERFORMANCE LEVEL.
- B. NO EFFECT.

Fig. 4. Effect on performance of heat losses from interior of thrust chamber

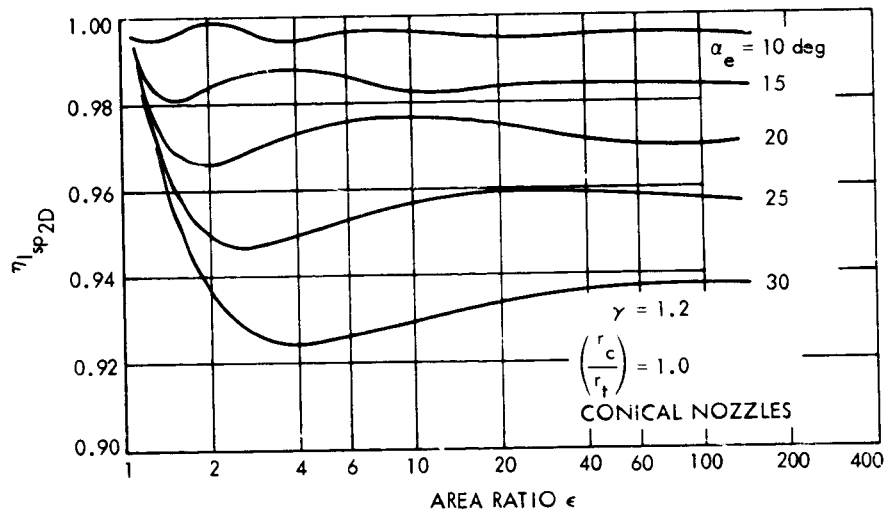


Fig. 5. Two-dimensional specific impulse efficiency for conical nozzles at $\gamma = 1.20$

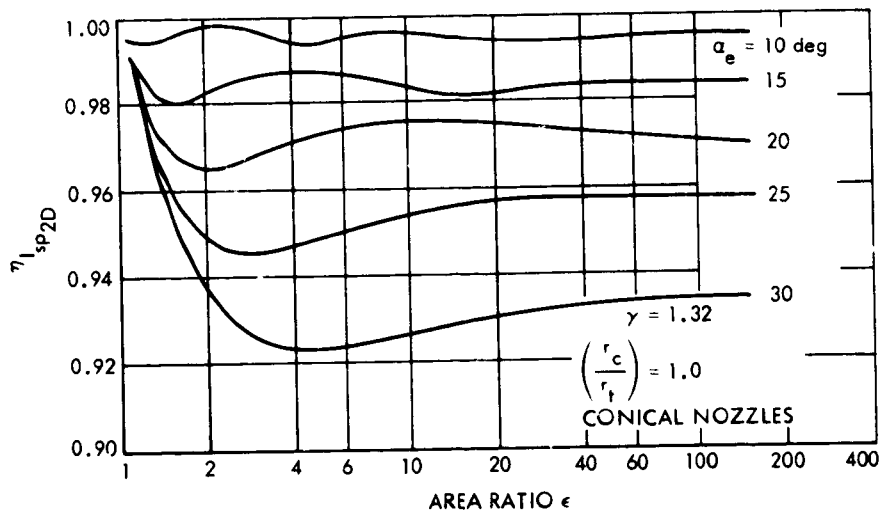


Fig. 6. Two-dimensional specific impulse efficiency for conical nozzles at $\gamma = 1.32$

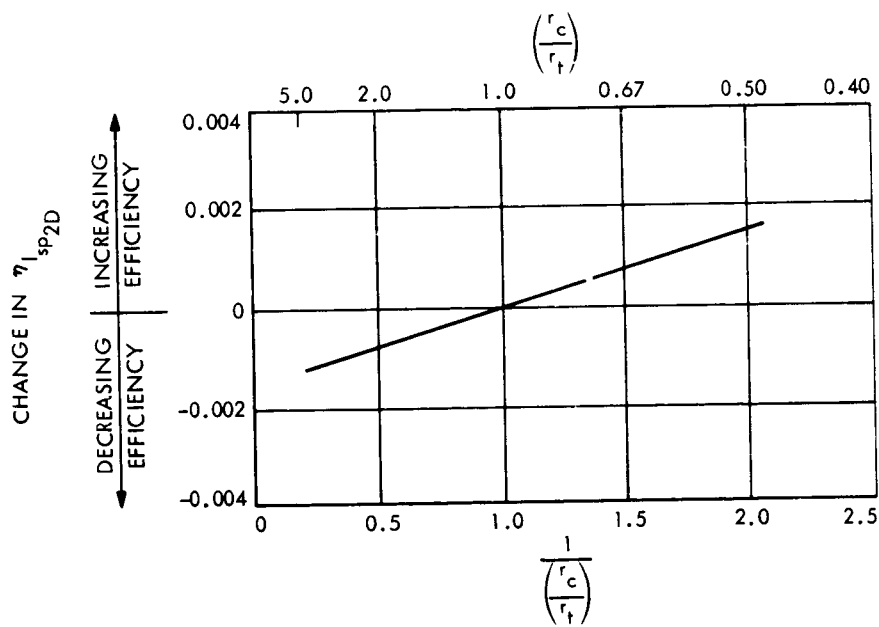


Fig. 7. Typical effect of throat wall radius of curvature on the two-dimensional specific impulse efficiency of conical nozzles

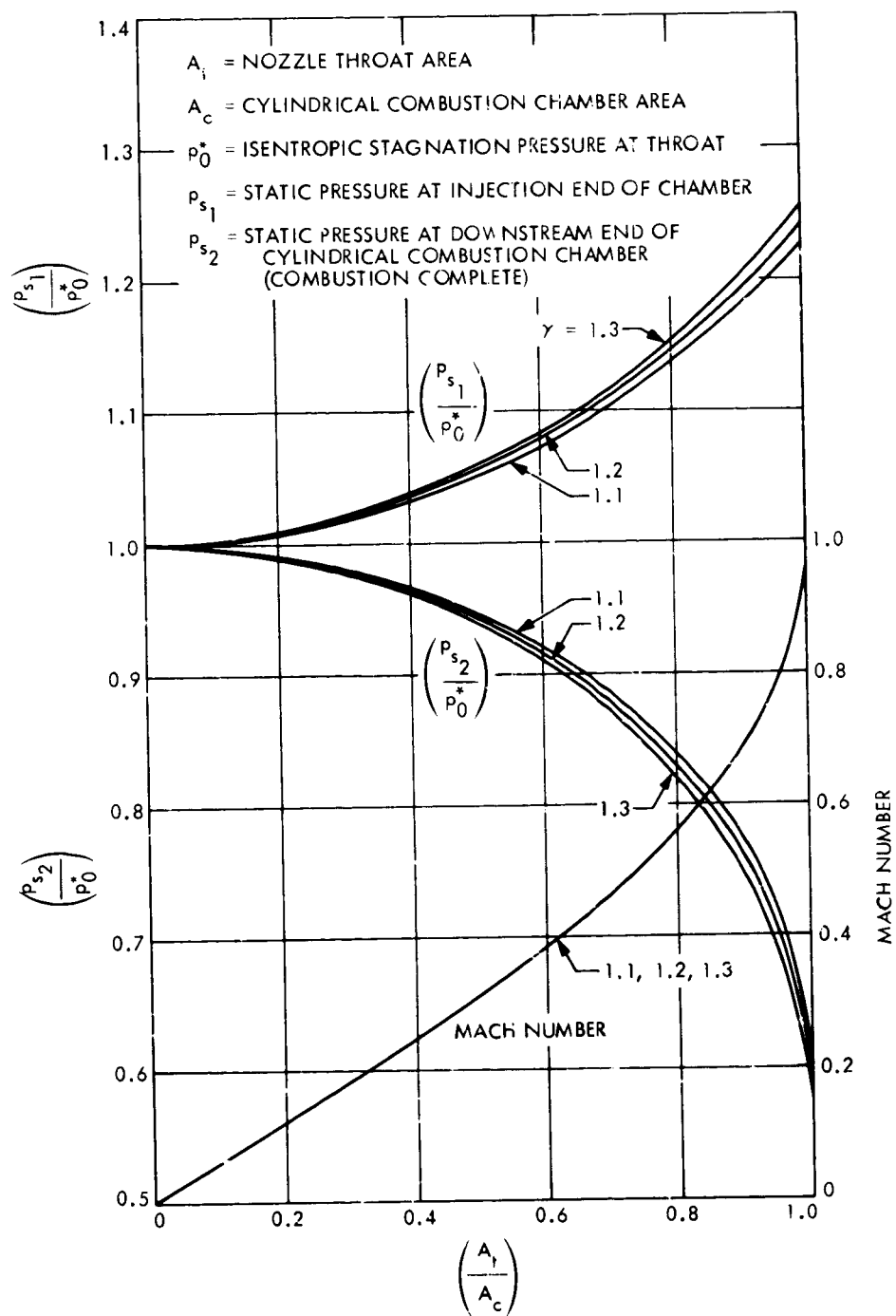


Fig. 8. Effect of combustion chamber area ratio on chamber static pressure at injection end and downstream end of cylindrical combustion chamber

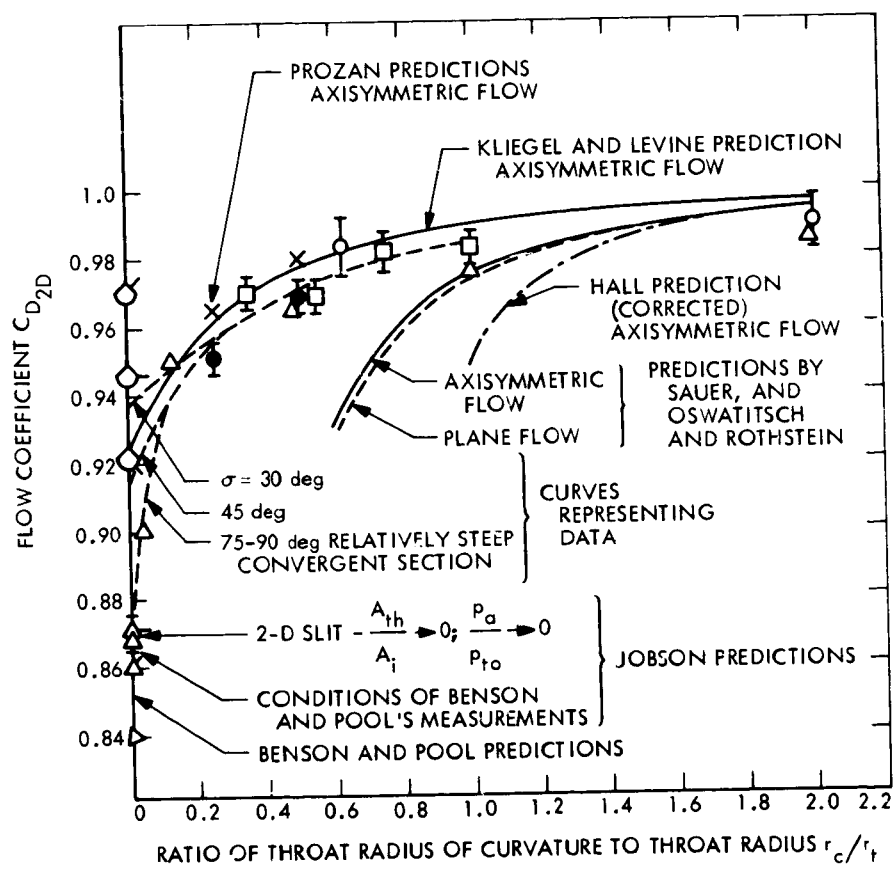


Fig. 9. Effect of nozzle throat radius of curvature on two-dimensional nozzle flow coefficient

CONFIGURATION	SOURCE	REF.*	$\frac{r_c}{r_{th}}$	r_{th} , in.	σ , deg	λ , deg	$Re_{D_{th}}$	$C_D = \frac{m}{m_{1D}}$
 <p>AXISYMMETRIC CONVERGENT-DIVERGENT NOZZLE</p>	● PRESENT RESULTS, JPL		0.25 0.49	0.800 ↓ 0.800	75 90	15 ↓	1.0×10^6 TO 4.0×10^6	0.951 ± 0.005 0.969 ± 0.005
	○ BACK, MASSIER AND GIER, JPL	6	0.625 2.0	0.800 0.902	45 30	15 ↓	1.8×10^6 TO 3.0×10^6	0.983 ± 0.008 0.990 ± 0.008
	□ NORTON AND SHELTON, JPL	5	0.35 0.55 0.75 1.0	0.563 ↓ 0.500	30 ↓ 45	15 ↓	5.9×10^6 TO 1.5×10^7	0.970 ± 0.005 0.969 ± 0.005 0.982 ± 0.006 0.983 ± 0.005
 <p>SHARP-EDGED ORIFICE</p>	△ DURHAM	3	0.04 0.125 0.50 1.0 2.0	0.500 ↓ 0.250	90 ↓ 45	15 ↓	$\sim 10^7$	0.900 0.950 0.965 0.976 0.985
	◇ BENSON AND POOL	14	→ 0	0.5	90	45	1.8×10^6	0.871 ± 0.005
	△ DURHAM △	15	→ 0 → 0	0.500 ↓ 0.250	90 90	45 0	$\sim 10^7$	0.860 0.870
 <p>SHARP THROAT CONICAL NOZZLE</p>	▷ PERRY	16	→ 0	0.156 TO 0.250	90	31	3.3×10^5 TO 5.2×10^5	0.840
	◁ THORNOCK	18	→ 0	1.50	15	90	$\sim 7 \times 10^6$ at $\frac{P_a}{P_t} = 0.14$ ($P_t = 100$ psia)	0.970
	◁ ◁		→ 0 → 0		25 40			0.946 0.922

*FROM REF 3 OF THIS PAPER.

Fig. 10. Explanation of data shown in Fig. 9

APPENDIX A
BOUNDARY-LAYER EFFECTS ON PERFORMANCE

Boundary-layer effects in rocket nozzle flow arise from friction and from heat transfer at the nozzle surface. Consider a simple one-dimensional axisymmetric flow as shown in Fig. A-1.

Far away from the wall, the flow is essentially inviscid and unaffected by the presence of the wall. In this region, it has "free-stream" values of pressure, temperature, velocity, and density. Near the wall the velocity and temperature profiles bend to match the values at the surface, as shown on Section AA and Section BB of Fig. A-1. The boundary-layer thickness δ is the distance from the wall at which there is no appreciable departure from free-stream conditions, either velocity or temperature; the static pressure is presumed to remain constant at the free-stream value throughout the boundary layer.

The boundary-layer displacement thickness δ^* is such that an inviscid free-stream flow extending from the axis out to the radial station $(r - \delta^*)$ would have the same mass flow as the real flow, with boundary layer, extending from the axis to the wall.

The boundary-layer momentum thickness θ is a measure of the excess of momentum which the equivalent inviscid flow has over the real flow: an inviscid free-stream flow extending from the axis out to $(r - \delta^* - \theta)$ would have the same momentum flux as the real flow, with boundary layer, extending from the axis to the wall.

Then, the thrust of the real flow is given by

- (1) The thrust of the equivalent inviscid flow through a real nozzle of contour $(r - \delta^*)$.

- (2) Less the excess momentum flux of the equivalent inviscid flow.
- (3) Plus the force exerted by the exit pressure on the annulus of width δ^* between the equivalent nozzle exit diameter and the real nozzle exit diameter.

In algebraic form, taking account of the nozzle exit divergence angle, as shown on Fig. A-2, and neglecting second-order terms, the thrust of a real nozzle can be written:

$$F = F_{\text{inviscid TDK}}^{\epsilon'} - \left[2\pi r_e \rho_e u_e^2 \theta_e \cos \alpha_e - 2\pi r_e p_e \delta_e^* \cos \alpha_e \right]_{\text{TDK}}^{\epsilon'} \quad (\text{A-1})$$

where the subscript ϵ' indicates that the calculations are made for inviscid flow through the equivalent nozzle contour.

This can be written in the form below, where it is equivalent to Eq. (4) of the text:

$$I_{sp} = \frac{1}{\dot{m}_t} F_{\text{inviscid TDK}}^{\epsilon'} - \left\{ \frac{2p_e A_e \cos \alpha_e}{\dot{m}_t} \left[\left(\frac{\rho_e u_e^2}{p_e} \right) \left(\frac{\theta_e}{r_e} \right) - \left(\frac{\delta_e^*}{r_e} \right) \right] \right\}_{\text{TDK}}^{\epsilon'} \quad (\text{A-2})$$

or

$$I_{sp} = I_{sp}^{\text{inviscid TDK}} - \Delta_1 I_{sp}^{\text{BL}} \quad (\text{A-3})$$

Then, following Eqs. (5), (6), (7), and (8) of the text, the expression for $\Delta_2 I_{sp}^{\text{BL}}$, to be used when the performance is referenced to an inviscid expansion through the geometrical nozzle contour, is developed.

Thus, as in Eq. (7) of the text,

$$I_{sp} = I_{sp}^{\text{TDK}} - \Delta_2 I_{sp}^{\text{BL}} \quad (\text{A-4})$$

and from Eqs. (5) and (8) of the text

$$\begin{aligned}
 \Delta 2I_{sp_{BL}} = & \left\{ \frac{2A_e p_e \cos \alpha_e}{\dot{m}_t} \left[\left(\frac{\rho_e u_e^2}{p_e} \right) \left(\frac{\theta_e}{r_e} \right) - \left(\frac{\delta_e^*}{r_e} \right) \right] \right\}_{\substack{\text{TDK} \\ \epsilon}} \\
 & + \frac{\partial}{\partial \epsilon} \left\{ \frac{2A_e p_e \cos \alpha_e}{\dot{m}_t} \left[\left(\frac{\rho_e u_e^2}{p_e} \right) \left(\frac{\theta_e}{r_e} \right) - \left(\frac{\delta_e^*}{r_e} \right) \right] \right\}_{\substack{\text{TDK} \\ \epsilon}} (\epsilon' - \epsilon) \\
 & - \frac{\partial}{\partial \epsilon} \left[\sum_{\substack{\text{sp}_i \\ \text{TDK} \\ (\text{O/F})_{i, \text{vap}}^* \\ \text{HL}}} I_{\substack{\text{sp}_i \\ \text{TDK} \\ (\text{O/F})_{i, \text{vap}}^* \\ \text{HL}}} \left(\frac{\dot{m}_{i, \text{vap}}^*}{\dot{m}_t} \right) \right]_{\epsilon} (\epsilon' - \epsilon) \quad (\text{A-5})
 \end{aligned}$$

where

$$(\epsilon' - \epsilon) = -2\epsilon \frac{\left[\left(\frac{\delta_e^*}{r_e} \right) \cos \alpha_e - \left(\frac{\delta_t^*}{r_t} \right) \right]}{\left(1 - 2 \frac{\delta_t^*}{r_t} \right)} \quad (\text{A-6})$$

At this point, the boundary-layer specific impulse loss would be evaluated by the following steps:

- (1) Use the TDK computer program to determine the overall performance and the properties (ρ , u , p , T , c_p , etc.) of the boundary flow stream tube.
- (2) Use the boundary stream-tube properties from TDK and a specification of wall temperature distribution as input to a

boundary-layer computer program (TBL, MA3L, BLIMP) and determine the boundary-layer thicknesses (θ_e/r_e) and (δ^*/r_e) .¹⁶

- (3) Use the output of the previous two steps to determine the rates of change with nozzle area ratio of the quantities in the last two terms of Eq. (A-5); this can be done graphically.
- (4) Use the results of steps (1), (2), and (3), above, in Eq. (A-5) to calculate the value of $\Delta_{2I_{sp}}^{BL}$.

The above calculation of the boundary-layer specific impulse correction is essentially a "reference methodology" calculation, as it requires the use of both the TDK and one of the boundary-layer computer programs. It is the intent of this report to develop a "simplified" performance calculation procedure which avoids the use of long-running and therefore expensive-to-use computer programs like TDK and, if possible, the various boundary-layer programs. This objective has been achieved up to the point of computing the boundary-layer loss. (All of the other components and losses of the performance are calculated or approximated with the use of only the ODE, TDE, and ODK computer programs.) It is now necessary to attempt to find feasible and acceptable approximations and simplifications for the evaluation of the boundary-layer correction.

As a first step in the simplification of Eq. (A-5), it is convenient to eliminate the mass flow rate in favor of the characteristic velocity. From Eqs. (26) and (27) of the text, the following equation can be written:

$$\frac{\bar{p}_0^* A_t}{\dot{m}_t} = \eta c_{TC}^* c_{ODE}^* (O/F)_{avg} \quad (A-7)$$

For further simplification, it can be assumed that the boundary-layer pressure, velocity, and density (and thus boundary-layer thicknesses) are

¹⁶The combustion gas recovery temperature and heat-transfer coefficient, the wall temperature, and the heat flux into the wall must be an internally consistent set. It may take several iterations with a heat-transfer program to achieve a heat balance and converge on the correct wall temperature for a regeneratively cooled thrust chamber.

- (3) Use TDE to compute boundary-layer stream properties (p_e , ρ_e , u_e , T_e , c_p , etc.).
- (4) Use a boundary-layer computer program to compute θ_e and δ_e^* .
- (5) Determine $\eta_{I_{sp}}^{2D}$ from available design charts and calculate or estimate

$$\eta_{I_{sp}}^{HL}, \eta_{I_{sp}}^{ER}, \text{ and } \eta_{c_{TC}}^*$$

- (6) Determine graphically the slopes occurring in the second and third terms of Eq. (A-8).

Examination of the relative magnitude of the three terms of Eq. (A-8) shows that the first term is predominant. The second and third terms are of opposite sign and become relatively negligible at high nozzle area ratio. Also, at high nozzle area ratio, the relative effect of the (δ_e^*/θ_e) factor in the first term decreases. At low area ratio, corresponding to "sea level" testing, all terms in Eq. (A-8) will have to be included in the calculations.

In the numerical evaluation of the first and second terms of Eq. (A-8), it is helpful to recognize that

- (1) The term $[\epsilon(p_e/p_0^*)(\rho_e u_e^2/p_e)]$ is relatively invariant, having a value of about 1.25 at $\epsilon = 2$ and increasing to about 1.8 at $\epsilon = 100$ (see Fig. A-3).
- (2) The term $(\rho_e u_e^2/p_e)$ varies from γ at the nozzle throat to from 20 to 50 at $\epsilon = 100$, depending on the value of γ (see Fig. A-4).

The evaluation of the boundary-layer specific impulse loss from Eq. (A-8), as described above, is a simplified direct calculation procedure which uses the most economical of the computer programs giving the needed output information, and is still based on the actual combustion product properties and the actual thrust chamber and nozzle size and shape.

An approximate boundary-layer specific impulse loss evaluation method is described in Ref. 1, Appendix B. This method uses charts based on calculations using the TBL boundary-layer program for typical thrust chamber nozzle shapes and over a range of wall temperatures and combustion gas properties. This method can be used to obtain rough estimates of the boundary-layer loss.

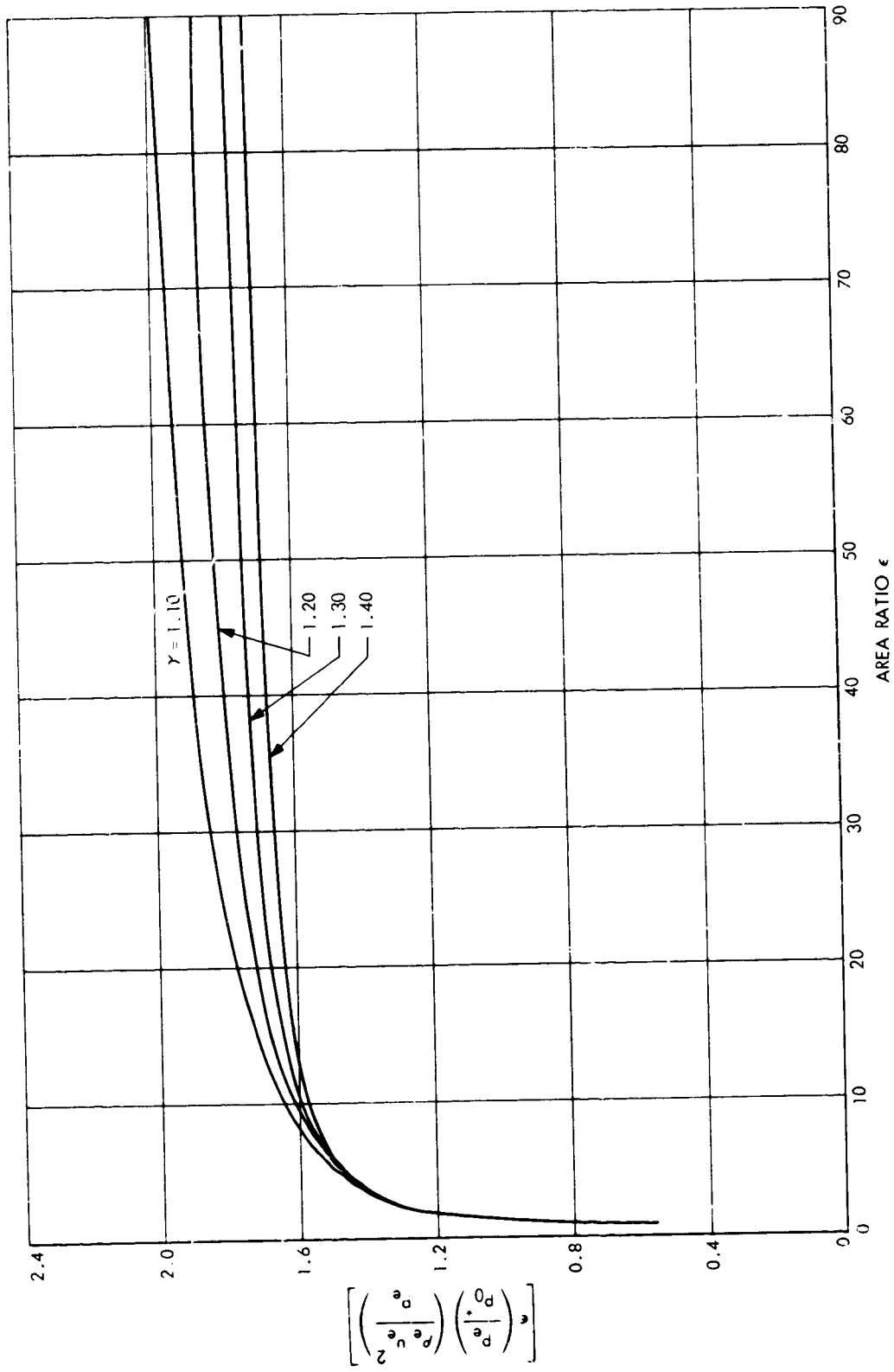


Fig. A-3. Perfect gas values of the thermodynamic function $[\epsilon(p_e/p_0)^*(\rho_e u_e^2/p_e)]$ used in calculating performance loss due to boundary-layer effects

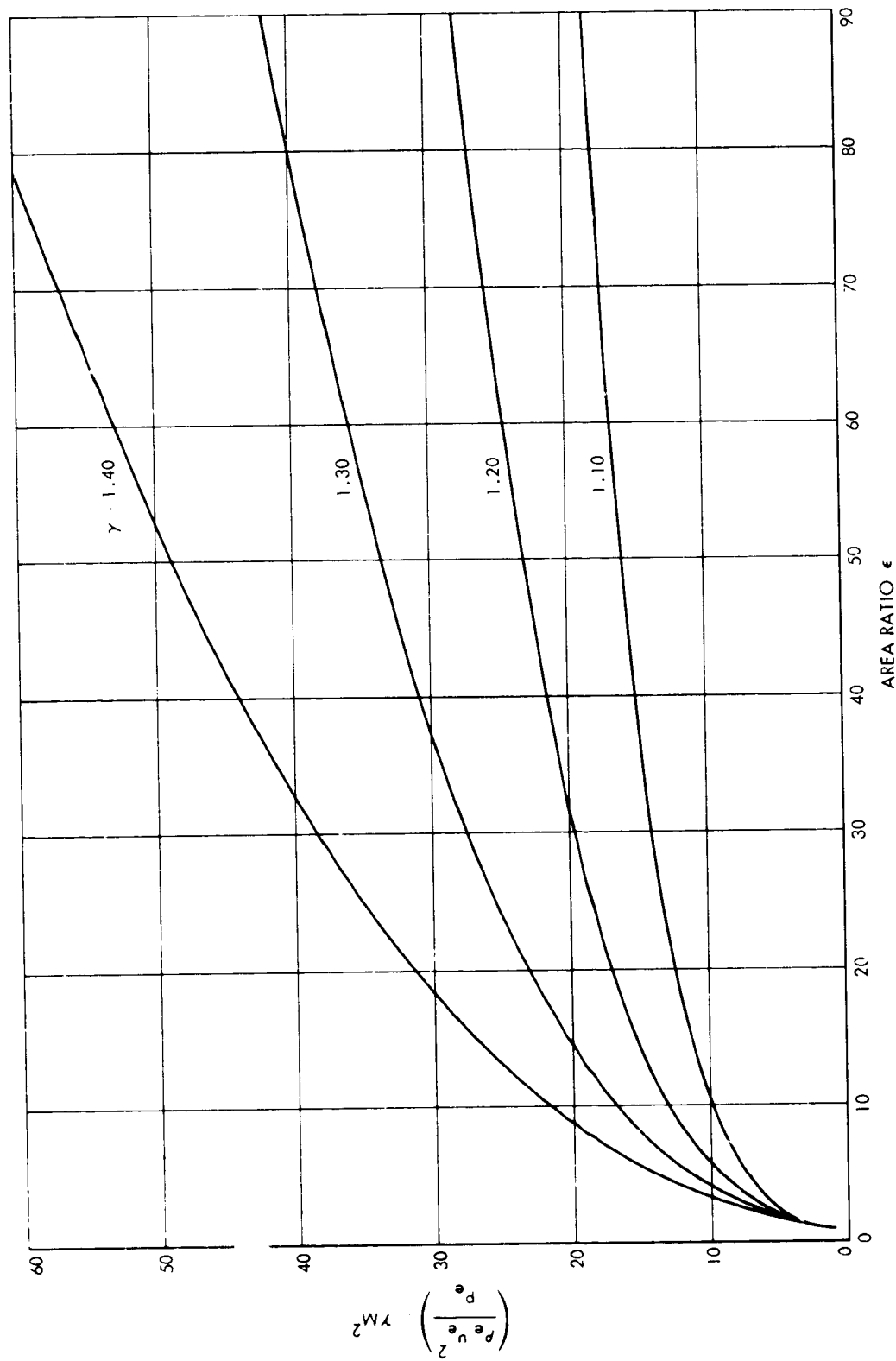


Fig. A-1. Perfect gas values of the thermodynamic function ($p_e u_e^2 / p_e$) used in calculating performance loss due to boundary-layer effects

APPENDIX B

FLOX-MMH PROPELLANT DATA

This appendix is presented as an example of the precalculations that can be performed for a given propellant, using the ODE and ODK computer programs. The propellant chosen as an example is the Flox (88% F₂-12% O₂) oxidizer with MMH fuel. The enthalpy of the propellant components (injection enthalpy) is as follows:¹⁸

Propellant component	Molecular weight, g/g-mol	Enthalpy, cal/g-mol	Temperature, K	Specific heat, cal/g-K
MMH (CH ₆ N ₂)	46.08	12700	298.15	0.6928
F ₂	38	-3100	90.20	0.363
O ₂	32	-3080	85.20	0.450

The performance calculations were made for a chamber pressure of 100 psia. Kinetic effects were determined at the scale of a 600-lbf thrust chamber (nozzle throat diameter = 2.00 in.).

The ODE computer program is used to determine enthalpy of the mixed propellant, the combustion temperature, the characteristic velocity, and the vacuum specific impulse as a function of propellant mixture ratio. The results of these calculations are shown in Figs. B-1 and B-2.

¹⁸ A set of recommended values of enthalpy, specific heat and density for various propellants is given in Appendix 2 of the Minutes of the Sixth Meeting of the JANNAF Performance Standardization Working Group, October 26-27, 1972, and is reproduced here as Table B-1.

Equivalent calculations are made with the ODK computer program, and the ratio of ODK to ODE values for characteristic velocity and specific impulse is plotted as kinetic efficiency in Fig. B-3.

The ODE calculations were repeated with higher and lower values of the propellant enthalpy in order to determine the change in characteristic velocity and specific impulse due to changes in injection enthalpy. The influence coefficients obtained from these calculations are given in Fig. B-4. These influence coefficients can be used, as described in the text, in accounting for differences in the total injection enthalpy from the values shown in the above tabulation, and in accounting for heat loss to the injector and chamber upstream of the boundary-layer attachment point.

In the absence of a good set of boundary-layer calculations for this propellant in the thrust chamber configuration shown in Appendix C, the boundary-layer specific impulse efficiency decrement was estimated as shown in Fig. B-5 for use in the sample performance data analysis.

Table B-1. Recommended heats of formation for propellants

Empirical Formula	Compound	Assigned Enthalpy		Temperature °K	Density g/cc	References	
		kcal/mol	kcal/100 gm			Enthalpy	Density
ClF ₅	Chlorine Pentafluoride (L)	-60.5±6.0	-46.4	298.15	1.779	1	1
	Cp(cal/gm-°K) = 0.1941 + 0.4824 × 10 ⁻³ (T,°K) over range 223-323°K (Ref. 2)						
ClF ₃	Chlorine Trifluoride (L)	-44.45±0.8	-48.08	298.15	1.807	1	1
	Cp(BTU/lb-°K) = 0.30939 - 1.672 × 10 ⁻⁴ (T,°R) + 3.0870 × 10 ⁻⁷ (T,°R) ² over range 355-500°R (Ref. 5)						
B ₂ H ₆	Diborane (L)	+4.97±4.0	+17.94	180.59	0.4371	1	1
F ₂	Fluorine (L)	-3.098±0.02	-8.153	85.02	1.505	1	1
	Cp(cal/mol-°K) = 13.8 @ 82°K (Ref. 2)						
N ₂ H ₄	Hydrazine (L)	+12.05	+37.60	298.15	1.0037	1	3
	Cp(cal/gm-°K) = 0.7356 @ 298°K Cp(cal/gm-°K) = 0.88415 - 1.3949 × 10 ⁻³ (T,°K) + 3.0074 × 10 ⁻⁶ (T,°K) ² (Ref. 3 anhydrous hydrazine)						
H ₂	Hydrogen (L)	-2.154±0.02	-106.8	20.27	0.0709	1	1
H ₂ O ₂	Hydrogen Peroxide (L)	-44.88±0.02	-131.9	298.15	1.44	1	2
	Cp(cal/gm-°K) = 0.628 average between 273 and 300°K						
H ₂ O _{1.8266}	90% Hydrogen Peroxide (L) 10% H ₂ O (L)	-45.01	-144.07	298.15	1.4136	2	2
	Cp(cal/gm-°K) = 0.660 average between 273 and 300°K, empirical formula assumes one mole solution						
CH ₄	Methane (L)	-21.39±0.10	-133.3	111.66	0.4239	1	1
CH ₃ N ₂	Monomethylhydrazine (L)	-12.9	+28.0	298.15	0.8702	4	3
	Ref. 2 recommends ΔH _{f298} ^o = 12.7 kcal/mol Ref. 3 recommends ΔH _{f298} ^o = 13.106 kcal/mol Cp(cal/gm-°K) = 0.6528 - 1.7284 × 10 ⁻⁵ (T,°K) + 3.9142 × 10 ⁻⁷ (T,°K) ² over range 226-360°K (Ref. 3)						
HNO ₃	Nitric Acid (L)	-41.46±0.10	-65.79	298.15	1.5027	1	1
	Cp(cal/gm-°K) = 0.4215 @ 298°K Cp(cal/mole-°K) = 25.64 + 1.427 × 10 ⁻² (T,°K) - 4.090 × 10 ⁻⁵ (T,°K) ² no temperature range given for heat capacity equation (Ref. 2)						
H _{0.8894} N _{0.9365} O _{2.699}	Red Fuming Nitric Acid RFNA (L)	-36.48	-63.81	298.15	1.55	2	2
	84% HNO ₃ /14% NO ₂ /2% H ₂ O, empirical formula assumes one mole solution						
N ₂ O ₄	Nitrogen Tetroxide (L)	-4.68±0.4	-5.08	298.15	1.431	1	1
	Cp(BTU/lb-°R) = 0.3696 @ 536.7°R Cp(BTU/lb-°R) = 0.24668 + 2.2880 × 10 ⁻⁴ (T,°R), Ref. 5 from 477 to 524°R						
O ₂	Oxygen (L)	-3.102±0.02	-9.694	90.18	1.149	1	1
	Cp(cal/gm-°K) = 0.4050 @ 90.18°K n.b.p. (Ref. 2)						
OF ₂	Oxygen Difluoride (L)	-8.38±0.90	-15.58	127.8	1.521	1	1
C ₂ H ₈ N ₂	unsym Dimethylhydrazine (L) UDMH	+11.9	+19.8	298.15	0.7861	1	3
	Ref. 3 recommends ΔH _{f298} ^o = 12.339 kcal/mol Cp(cal/gm-°K) = 0.653 @ 298°K (Ref. 2) Cp(cal/gm-°K) = 0.4071 + 8.838 × 10 ⁻⁴ (T,°K) over range 216-335°K by Ref. 3 but values considered "provisional"						
C _{0.6956} H _{5.3911} N _{2.0}	Aerozine 50; 50% UDMH/50% N ₂ H ₄ (L)	+12.31	+29.45	298.15	0.8987	3	3
	Enthalpy obtained by molar addition of N ₂ H ₄ (0.6522 mole) and UDMH (0.3478 mole) plus heat of mixing Cp(cal/gm-°K) = 0.732 @ 298°K Cp(cal/gm-°K) = 0.5124 + 7.3624 × 10 ⁻⁴ (T,°K) over range 275-323°K (Ref. 3), empirical formula assumes one mole solution						

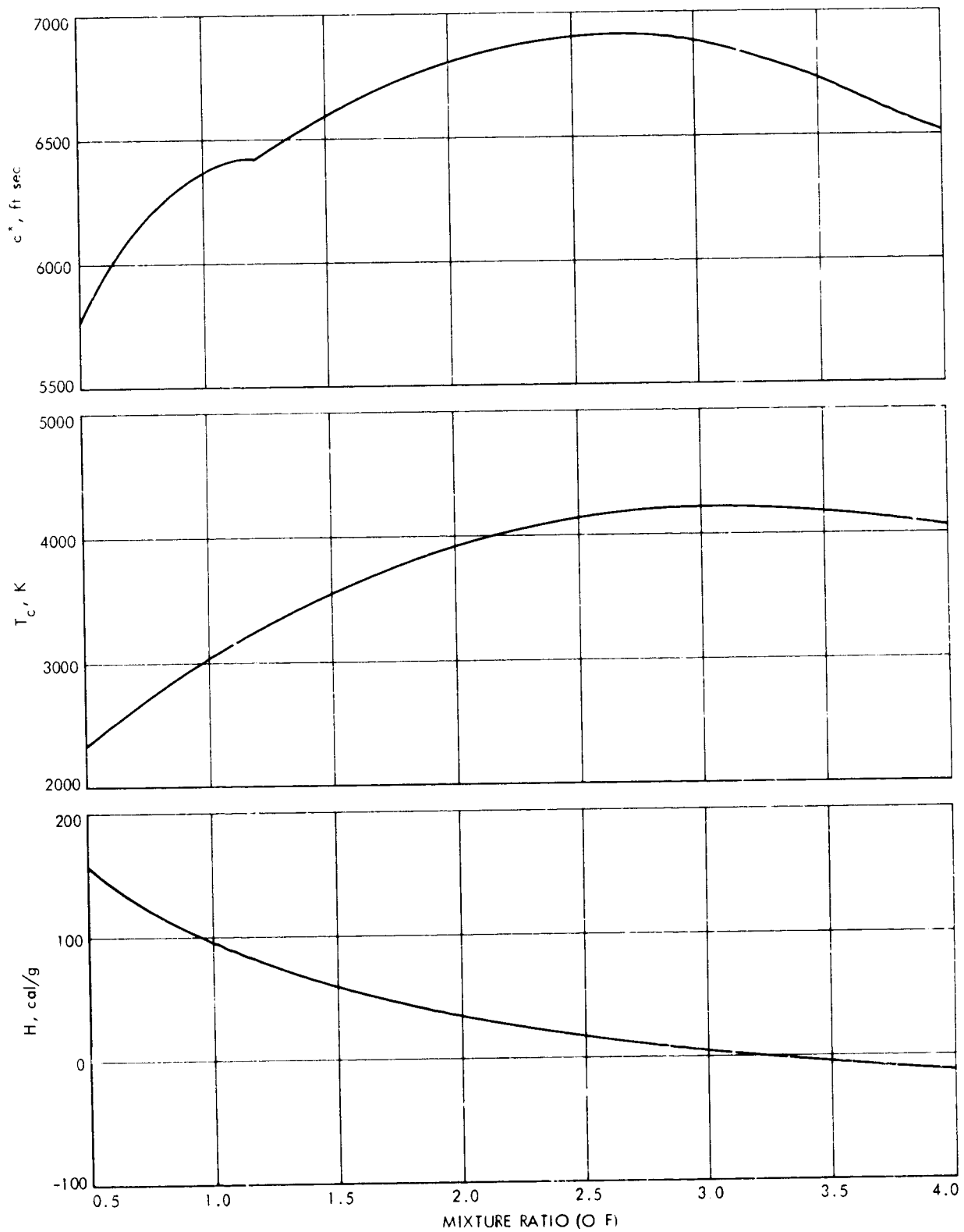


Fig. B-1. ODE reference performance for Flox (88-12)-MMH (enthalpy, chamber temperature, characteristic velocity)

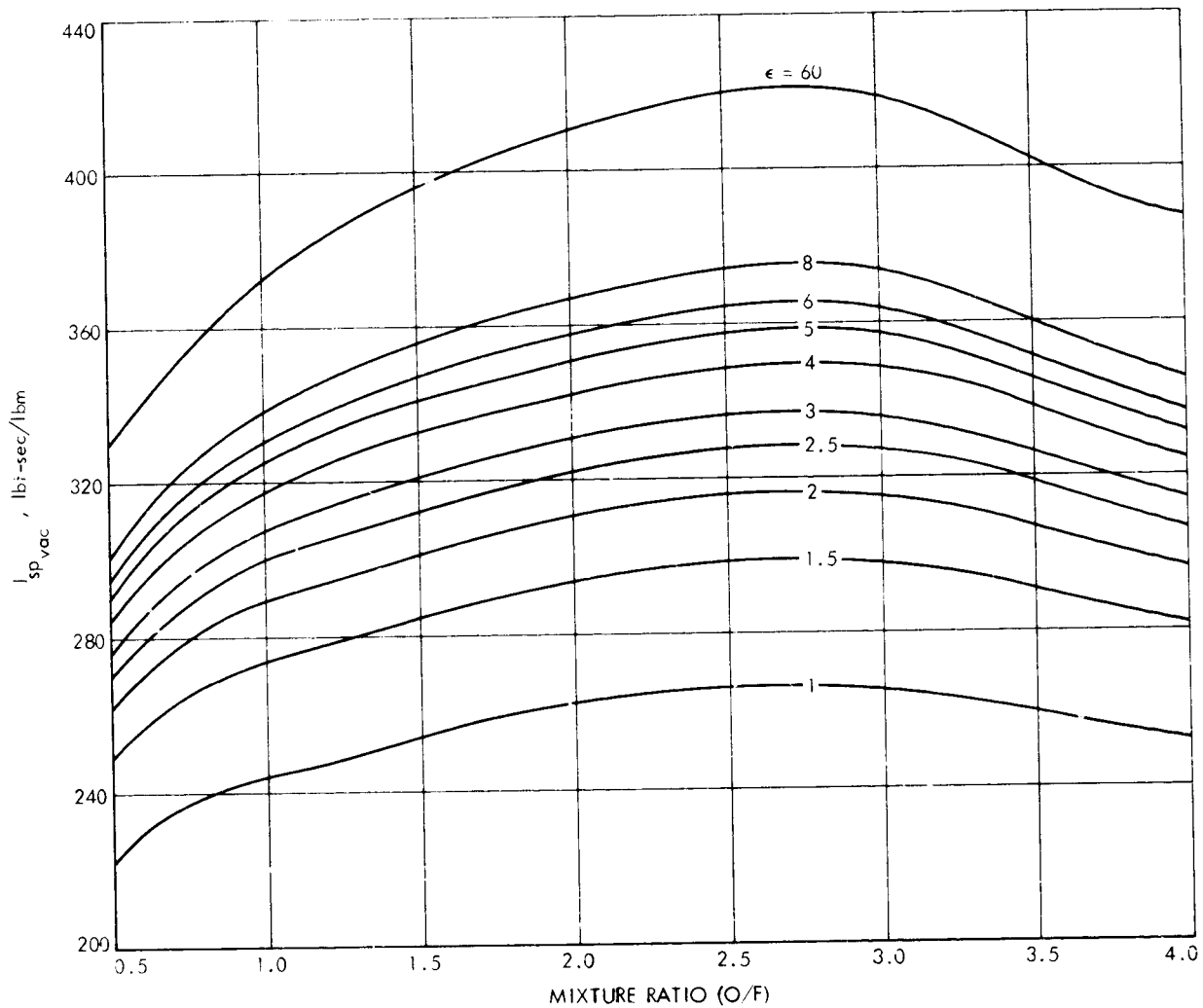


Fig. B-2. ODE reference performance for Flox (88-12)-MMH (vacuum specific impulse vs nozzle area ratio)

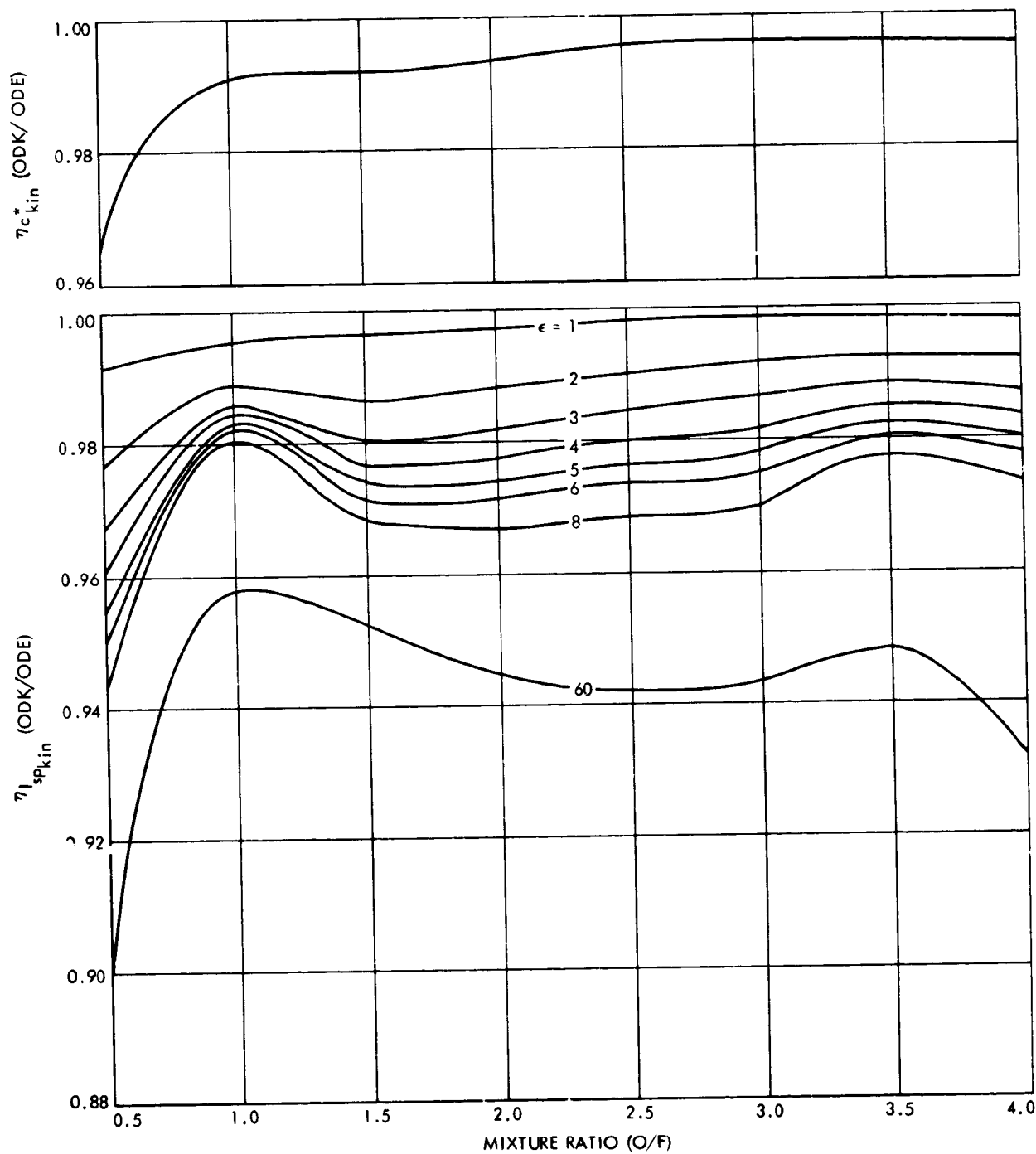


Fig. B-3. Kinetic efficiency factors for Flox (88-12)-MMH

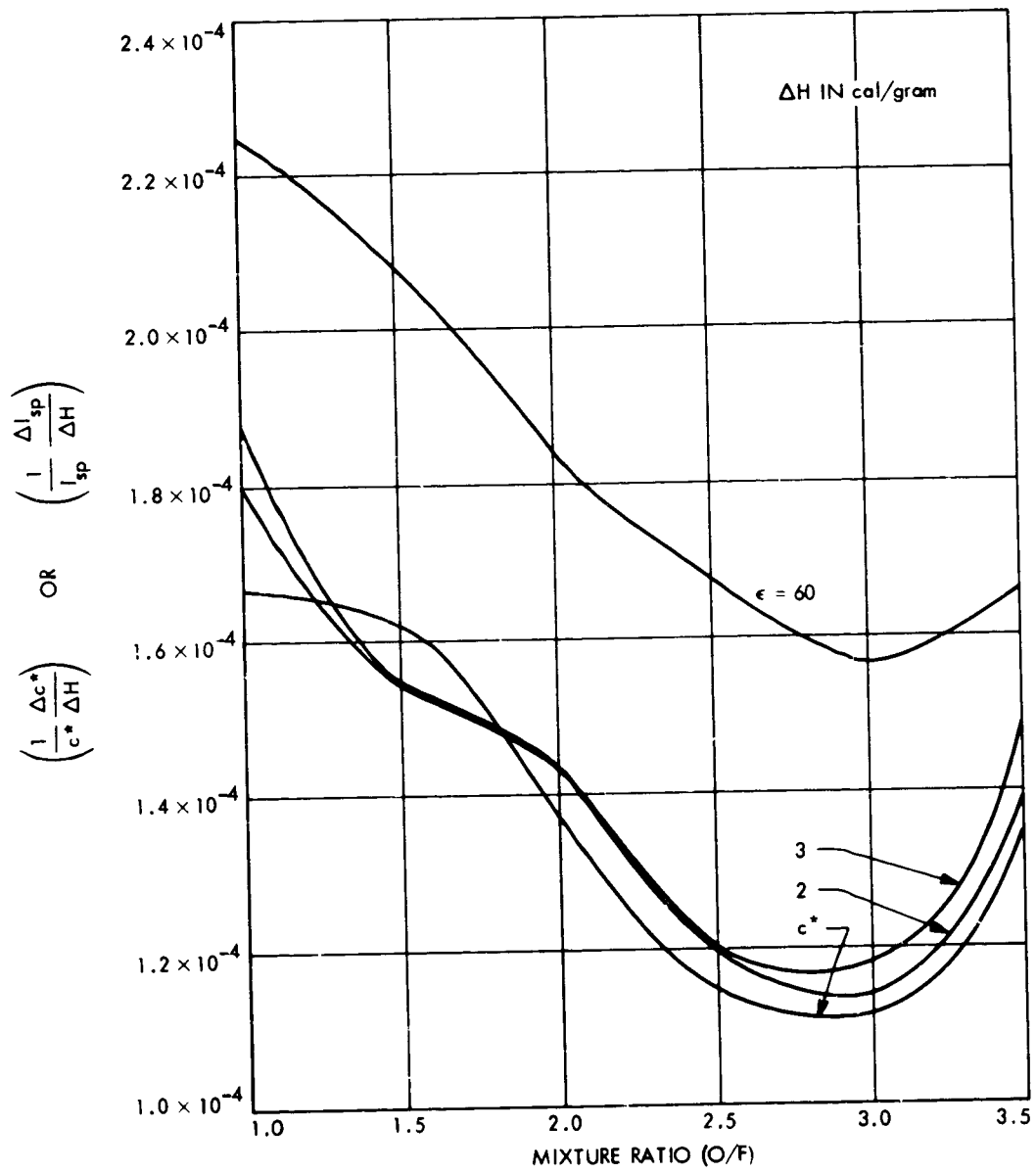


Fig. B-4. Effect of injection enthalpy change on performance of Flox (88-12)-MMH

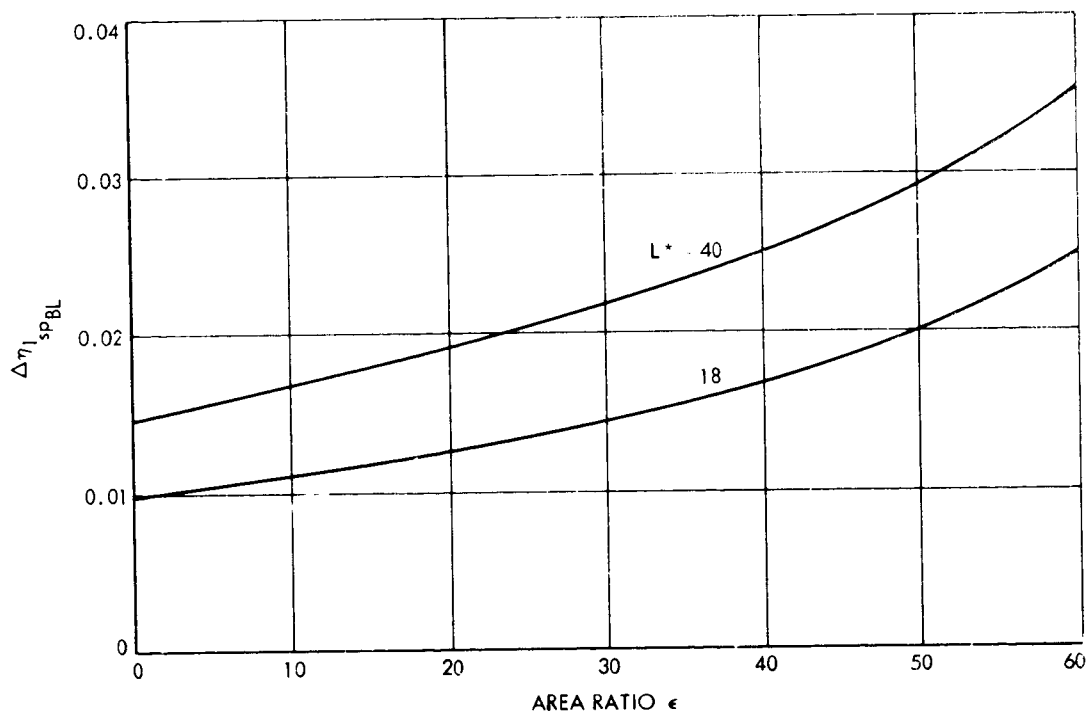


Fig. B-5. Boundary-layer loss estimate for 600-lbf thrust chamber

APPENDIX C

EXAMPLE CORRELATION AND EXTRAPOLATION OF FLOX-MMH TEST DATA

The methods of thrust chamber performance correlation and prediction developed and discussed in the preceding portions of this report are applied here, as an example, to experimental data obtained at the Jet Propulsion Laboratory.

The experimental data was obtained during tests leading to the development of a 600-lbf vacuum thrust rocket motor utilizing Flox (88-12)-MMH as propellant. The test motor had a copper heat-sink thrust chamber with a nozzle exit-area ratio of $\epsilon = 2.50$, and was operated at a chamber pressure (nozzle throat stagnation pressure) of approximately 100 psia.

Data from a number of tests made over a range of mixture ratio were plotted versus mixture ratio, and the performance values used here for the example correlation were read at a mixture ratio of $(O/F) = 2.20$ from curves faired through the plotted data points; these performance values are given in the labeled box in Table C-1.

Table C-1 shows performance data for two different thrust chamber lengths, corresponding to L^* values of 18 and 40 in. Comparison of these two sets of data and the corresponding performance efficiency factors clearly shows that the combustion and energy release is more complete in the longer thrust chamber. The right-hand column of Table C-1 shows the extrapolation of the efficiency factors obtained by correlation of the $\epsilon = 2.5$ test data to a thrust chamber with a nozzle exit-area ratio of $\epsilon = 60$, and the predicted specific impulse at this area ratio.

The correlation of the experimental data and the prediction of the performance with the $\epsilon = 60$ nozzle are obtained by the following steps:

(1) Correlation of $\epsilon = 2.5$ test data

- (a) Enter in the table the "reference" equilibrium performance of the propellant at the overall average mixture ratio, as given in Appendix B, Figs. B-1 and B-2.
- (b) Correct this "reference" performance for the difference of the actual propellant component injection temperatures and enthalpies, compared to the "reference" values, as listed in Appendix B. This is done using the injection enthalpy influence coefficient curve (Fig. B-4). The sample calculations are given as Appendix D.
- (c) Compare the measured delivered performance with the ODE equilibrium performance for the propellant at the actual injection enthalpy to obtain the thrust chamber performance efficiencies (Eqs. 2 and 25 of the text).
- (d) Compute the performance efficiency due to the heat loss from the injector face and the portion of the chamber upstream of the boundary-layer attachment point, using Eqs. (10) and (32) of the text and the influence coefficients from Fig. B-4. In this case it is assumed that 3 in. of chamber length is involved, and that the heat flux in this region is $q = 1.0 \text{ Btu/in.}^2\text{-sec.}$ The details of this calculation are given in Appendix E.
- (e) The efficiency factor for two-dimensional flow through the nozzle is read directly from Fig. 5 or 6 for specific impulse, and obtained from Fig. 9 and Eq. (28) of the text for characteristic velocity.
- (f) The efficiency factors resulting from kinetic loss at the overall average mixture ratio are read directly from Fig. B-3.
- (g) The effect of friction and heat loss from the attached boundary-layer region on specific impulse is taken from

the estimated curves of Fig. B-5. The effect of the boundary-layer loss on characteristic velocity is assumed to be $\eta_{c_{HL}}^* = 1.002$, corresponding to the assumption that $(\delta_t^*/r_t) = 0.001$ (cf Eq. 33 of the text).

- (h) The energy-release efficiency is then "backed out" from the measured overall thrust chamber efficiencies and the other component efficiencies evaluated above, using Eqs. (23) and (35) of the text.

(2) Extrapolation to performance at $\epsilon = 60$

- (a) The predicted specific impulse at $\epsilon = 60$ for the propellant at its actual injected enthalpy is found as before, using Figs. B-1, B-2, and B-4. The associated calculations are given in Appendix D.
- (b) The injector and chamber upstream-end heat loss specific impulse performance efficiency is obtained as before from Eq. (10) and the influence coefficient given in Fig. B-4. The calculational details are given in Appendix E.
- (c) The two-dimensional flow effect on specific impulse at $\epsilon = 60$ is obtained directly from Figs. 5 and 6 of the text.
- (d) The kinetic efficiency factor for specific impulse at $\epsilon = 60$ is obtained directly from Fig. B-3.
- (e) The boundary-layer effect on specific impulse at $\epsilon = 60$ is obtained from the curve in Fig. B-5.
- (f) The energy release efficiency at $\epsilon = 60$ is conservatively assumed to be the same as at $\epsilon = 2.5$.
- (g) The overall thrust chamber specific impulse efficiency at $\epsilon = 60$ is then calculated from the component efficiencies, using Eq. (16) of the text.
- (h) The predicted, or extrapolated, vacuum specific impulse at $\epsilon = 60$ is obtained by multiplying the ODE specific impulse by the overall thrust chamber specific impulse efficiency factor calculated above, as per Eq. (15) of the text.

The results of the data correlation are summarized in the first two columns of Table C-1; it is found here that the characteristic velocity energy-release efficiency is very nearly equal to the overall thrust chamber characteristic velocity efficiency. For this particular example, too, the specific impulse energy release efficiency at $(O/F) = 2.2$ and at $\epsilon = 2.5$ is very close to the characteristic velocity energy-release efficiency.

Table C-1. Test data and efficiency factor correlation for tests of 600-lbf Flox (88-12)-MMH thrust chamber with $\epsilon = 2.5$ nozzle area ratio and extrapolation to performance at $\epsilon = 60$ nozzle area ratio

Parameters	Test conditions		Extrapolation
L_n , in.	18	40	40
(O/F)	2.2	2.2	2.2
ϵ	2.5	2.5	60
I_{sp} , lbf-sec/lbm	325	325	417
c_{ODE}^* , ft/sec	6875	6875	6875
I_{sp} , lbf-sec/lbm	325	325	417
c_{ODE}^* , ft/sec	6875	6875	6875
	Crossplotted test data		Predicted
I_{sp} , lbf-sec/lbm	290	295.2	354
c^* , ft/sec	6305	6340	
η_{sp}	0.892	0.938	0.848
η_{TC}	0.998	0.998	0.998
η_{sp} _{HL}	0.985	0.985	0.985
η_{sp} _{2D}	0.980	0.980	0.944
I_{sp} _{kin}			0.935
ΔI_{sp} _{BL} (estimated)	0.010	0.015	
	Derived: backed out		
I_{sp} _{ER}	0.936	0.952	0.952
η_{TC} _{exp}	0.917	0.951	
η_{HL}	0.998	0.998	
η_{2D}	1.005	1.005	
η_{kin}	0.995	0.995	
η_{BL} (estimated)	1.002	1.005	
	Derived: backed out		
η_{ER}	0.917	0.948	

APPENDIX D

CORRECTION OF ODE PERFORMANCE FOR CHANGE IN PROPELLANT INJECTION TEMPERATURE

The change in performance due to changes in propellant injection temperature is obtained by determining the equivalent change in propellant injection enthalpy, and then using the precalculated enthalpy change influence coefficients given in Fig. B-4.

The "reference" ODE performance was computed for the propellant component temperatures given in Appendix B. These temperatures and the average temperatures of the propellant during the test program are given below:

Propellant component	Standard temperature, K	Test temperature, K	ΔT, K
MMH (CH ₆ N ₂)	298.15	308.0	+10.0
F ₂	90.20	82.0	-7.8
O ₂	85.20	82.0	+3.2

The total change in enthalpy, per unit mass of total propellant, is obtained by summing mass fractions of the propellant components times their specific heat and temperature change. Thus,

$$\Delta H = \sum_i \left[\frac{\dot{m}_i}{\dot{m}_t} c_{p_i} \Delta T_i \right]$$

for each propellant component.

The mass fractions of the propellant components at a mixture ratio of (O/F) = 2.20 are obtained as follows:

$$(O/F) \equiv r$$

$$\left(\frac{\dot{m}_{\text{oxidizer}}}{\dot{m}_t} \right) = \frac{r}{(r+1)} = \frac{2.2}{3.2} = 0.688$$

Since the oxidizer is 88% F₂ and 12% O₂

$$\left(\frac{\dot{m}_i}{\dot{m}_t} \right)_{F_2} = 0.88 \times 0.688 = 0.605$$

$$\left(\frac{\dot{m}_i}{\dot{m}_t} \right)_{O_2} = 0.12 \times 0.688 = 0.0825$$

$$\left(\frac{\dot{m}_{\text{fuel}}}{\dot{m}_t} \right) = \frac{1}{(r+1)} = \frac{1}{3.2} = 0.312 = \left(\frac{\dot{m}_i}{\dot{m}_t} \right)_{\text{MMH}}$$

Then, using the specific heats given in Appendix B,

$$\begin{aligned} \Delta H &= \Delta H_{F_2} + \Delta H_{O_2} + \Delta H_{\text{MMH}} \\ &= [0.605 \times 0.363 \times (-7.8) + 0.0825 \times 0.450 \times 3.2 \\ &\quad + 0.313 \times 0.6928 \times 10.0] \text{ cal/g} \\ &= +0.572 \text{ cal/g of total propellant} \end{aligned}$$

Then, from Fig. B-4 for $(O/F) = 2.2$,

$$\left(\frac{1}{c^*} \frac{\Delta c^*}{\Delta H} \right) = 1.25 \times 10^{-4} \frac{1}{\text{cal/g}}$$

$$\left(\frac{1}{I_{sp}} \frac{\Delta I_{sp}}{\Delta H} \right)_{\epsilon=2.5} = 1.33 \times 10^{-4} \frac{1}{\text{cal/g}}$$

$$\left(\frac{1}{I_{sp}} \frac{\Delta I_{sp}}{\Delta H} \right)_{\epsilon=60} = 1.765 \times 10^{-4} \frac{1}{\text{cal/g}}$$

and the corresponding values of performance change are

$$\frac{\Delta c^*}{c^*} = 1.25 \times 10^{-4} \times 0.572 = 0.0000715$$

$$\left(\frac{\Delta I_{sp}}{I_{sp}} \right)_{\epsilon=2.5} = 1.33 \times 10^{-4} \times 0.572 = 0.0000760$$

$$\left(\frac{\Delta I_{sp}}{I_{sp}} \right)_{\epsilon=60} = 1.765 \times 10^{-4} \times 0.572 = 0.000101$$

These values are completely negligible, so Table C-1 shows the ODE performance corresponding to the injection enthalpy as being identical to the performance at the reference enthalpy.

APPENDIX E

CALCULATION OF INJECTOR REGION HEAT LOSS EFFECTS

Heat loss to the downstream portion of the combustion chamber and in the contraction and expansion portions of the nozzle is accounted for in the boundary-layer performance efficiency loss factor. There is an effective starting point, or boundary-layer attachment point, beyond which the boundary-layer processes will adequately predict the measured heat loss. Upstream of this effective starting point, in the injection region, there is considerable large-scale turbulence, and the heat transfer is not described by the normal boundary-layer relationships. The effect on thrust chamber performance of the heat loss from the region upstream of the effective attachment point of the boundary layer must be accounted for separately from the boundary-layer loss accounting.

This appendix illustrates the method of calculating the effect of injector-region heat loss on thrust chamber performance. The configuration of the test chamber is shown in Fig. E-1. It is assumed that the effective attachment point of the boundary layer is 3 in. downstream of the injector face, and that the injector face and the chamber wall in the region upstream of the attachment point have a heat flux of 1.0 Btu/in.²-sec.

The total surface area included for injection-region heat loss is

$$A = \frac{\pi}{4} \times (3)^2 + \pi \times 3 \times 3 = 7.075 + 28.3 = 35 \text{ in.}^2$$

The heat flux in this region is

$$\dot{Q} = 35 \text{ in.}^2 \cdot 1.0 \text{ Btu/in.}^2\text{-sec} = 35 \text{ Btu/sec}$$

The total propellant mass flow into the chamber is given by

$$\dot{m}_t = \frac{p_0 A_t}{\eta_{c_{TC}^*} c_{ODE}^*} = \frac{100 \text{ (lb/in.}^2) \times \frac{\pi}{4} (2)^2 \text{ (in.}^2) \times 32.174 \text{ (lbm-ft/lbf-sec}^2)}{0.95 \times 6875 \text{ (ft/sec)}} = 1.55 \text{ lbm/sec}$$

where the value of $\eta_{c_{TC}^*} = 0.95$ is assumed.

It is assumed that, because of the turbulence in the injector region, the heat is lost uniformly from the total propellant. Then the equivalent enthalpy change of the propellant is

$$\Delta H_{HL} = \frac{\dot{Q}}{\dot{m}_t} = \frac{35 \text{ Btu/sec}}{1.55 \text{ lbm/sec}} = 22.6 \text{ Btu/lbm} = 12.55 \text{ cal/g}$$

From Fig. B-4 the injection enthalpy change performance influence coefficients at (O/F) = 2.2 are

$$\left(\frac{1}{c^*} \frac{\Delta c^*}{\Delta H} \right) = 1.25 \times 10^{-4} \frac{1}{\text{cal/g}}$$

$$\left(\frac{1}{I_{sp}} \frac{\Delta I_{sp}}{\Delta H} \right)_{\epsilon=2.5} = 1.33 \times 10^{-4} \frac{1}{\text{cal/g}}$$

$$\left(\frac{1}{I_{sp}} \frac{\Delta I_{sp}}{\Delta H} \right)_{\epsilon=60} = 1.765 \times 10^{-4} \frac{1}{\text{cal/g}}$$

The corresponding performance changes are

$$\frac{\Delta c^*}{c^*} = 1.25 \times 10^{-4} \times 12.55 = 0.00157$$

$$\left(\frac{\Delta I_{sp}}{I_{sp}} \right)_{\epsilon=2.5} = 1.33 \times 10^{-4} \times 12.55 = 0.00167$$

$$\left(\frac{\Delta I_{sp}}{I_{sp}}\right)_{\epsilon=60} = 1.765 \times 10^{-4} \times 12.55 = 0.00221$$

and the corresponding performance efficiency factors are

$$\eta_{c_{HL}^*} = \left(1 - \frac{\Delta c^*}{c^*}\right) = 0.9984$$

$$\eta_{I_{sp_{HL}}} = \left(1 - \frac{\Delta I_{sp}}{I_{sp}}\right) = 0.9983 \quad \text{at } \epsilon = 2.5$$

$$\eta_{I_{sp_{HL}}} = \left(1 - \frac{\Delta I_{sp}}{I_{sp}}\right) = 0.9978 \quad \text{at } \epsilon = 60$$

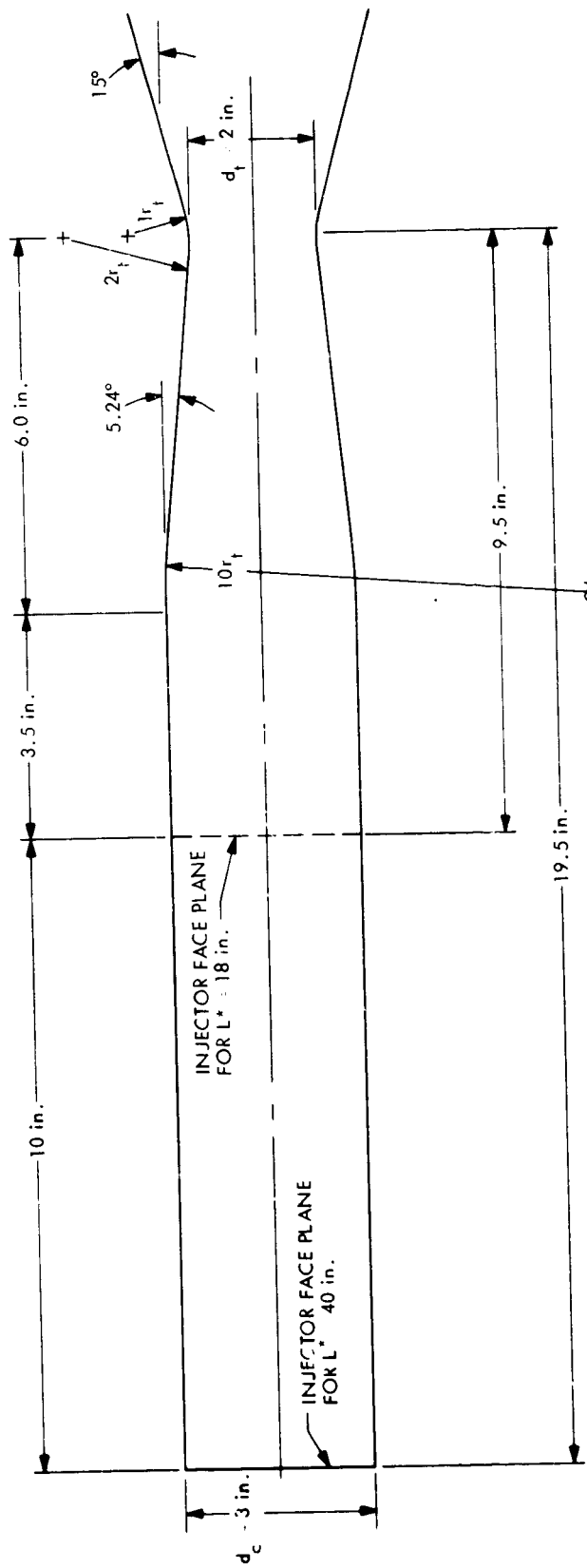


Fig. E-1. Experimental thrust chamber configuration

NOMENCLATURE

A_e	geometric nozzle-exit area under firing conditions
A_i^*	throat area of individual stream tube
A_{lip}	nozzle-exit lip area
A_t	geometric nozzle throat area under firing conditions
c^*	characteristic velocity - mass-flow parameter
C_D $2D$	discharge coefficient for throat curvature effects
F_{amb}	thrust measured with external pressure p_a
F_{vac}	thrust in vacuum environment
ΔF_{BL}	boundary-layer correction to calculated thrust
ΔF_{drops}	droplet contribution to total thrust
H_{inj}	injection enthalpy of propellant
I_{sp} vac	vacuum specific impulse
\dot{m}_i^*	mass-flow rate in one stream tube
$\dot{m}_{i, drop}^*$	mass-flow rate of unevaporated droplets remaining at stream-tube throat
$\dot{m}_{i, vap}^*$	evaporated mass-flow rate at stream-tube throat
\dot{m}_t	total mass-flow rate
$(O/F)_{avg}$	overall average injected mixture ratio of propellant
$(O/F)_{i, inj}$	injected mixture ratio in one stream tube
$(O/F)_{i, vap}^*$	mixture ratio of evaporated propellant at stream-tube throat
p_a	ambient pressure
p_e	pressure in boundary layer at nozzle exit
p_{s_x}	static pressure at wall of combustion chamber at axial location x
$p_{0_i}^*$	stagnation pressure at throat of stream tube (isentropic)

NOMENCLATURE (contd)

\bar{p}_0^*	average stagnation pressure at throats of stream tubes (defined)
\dot{Q}	rate of heat transferred to chamber upstream of boundary-layer attachment point (see subscript HL)
r_c	radius of curvature of nozzle throat
r_e	geometric radius of nozzle exit
r_t	geometric radius of nozzle throat
u_e	velocity, stream property at nozzle exit near wall
α_e	divergence angle of nozzle wall at exit
γ	ratio of specific heats of gas
δ_e^*	displacement thickness of boundary layer at nozzle exit
δ_t^*	displacement thickness of boundary layer at throat
Δ_{cor}	correlation coefficient for experimental vs. predicted performance
ϵ	nozzle exit-area ratio
$\eta_{c_{BL}}^*$	characteristic velocity efficiency accounting for boundary-layer friction and heat-transfer effects
$\eta_{c_{kin}}^*$	kinetic characteristic velocity efficiency
$\eta_{c_{(O/F)dist}}^*$	mixture-ratio distribution characteristic velocity efficiency
$\eta_{c_{TC_{exp}}^*}$	$= \frac{c_{exp}^*}{c_{ODE}^* (O/F)_{avg}}$
$\eta_{c_{TC_{pred}}^*}$	$= \frac{c_{pred}^*}{c_{ODE}^* (O/F)_{avg}}$
$\eta_{c_{HL}}^*$	characteristic velocity efficiency accounting for heat lost to the system upstream from the boundary-layer attachment point

NOMENCLATURE (contd)

$\eta_{c\text{vap}}^*$	droplet vaporization characteristic velocity efficiency
η_{c2D}^*	two-dimensional characteristic velocity efficiency
$\eta_{I\text{sp}}^{\text{kin}}$	kinetic specific impulse efficiency
$\eta_{I\text{sp}}^{\text{(O/F)dist}}$	mixture-ratio distribution specific impulse efficiency
$\eta_{I\text{sp}}^{\text{TC exp}}$	$= \frac{I_{\text{sp}}^{\text{vac exp}}}{I_{\text{sp}}^{\text{ODE (O/F)avg}}}$
$\eta_{I\text{sp}}^{\text{TC pred}}$	$= \frac{I_{\text{sp}}^{\text{vac pred}}}{I_{\text{sp}}^{\text{ODE (O/F)avg}}}$
$\eta_{I\text{sp}}^{\text{HL}}$	specific impulse efficiency accounting for heat lost to the system upstream from the boundary-layer attachment point
$\eta_{I\text{sp}}^{\text{vap}}$	droplet vaporization specific impulse efficiency
$\eta_{I\text{sp}}^{\text{2D}}$	two-dimensional-flow specific impulse efficiency
$\Delta\eta_{I\text{sp}}^{\text{BL}}$	specific impulse efficiency increment due to boundary-layer friction and heat transfer
θ_e	momentum deficiency thickness of boundary layer at nozzle exit
ρ_e	density, stream property at nozzle exit near wall

NOMENCLATURE (contd)

Subscripts

BL	boundary-layer loss effects
drops	unevaporated liquid droplets
e	nozzle exit
exp	experimental value, based on measured data
ER	effects due to incomplete energy release
i	individual stream-tube values
inj	corresponding to injected mass or mixture ratio
kin	effects due to finite reaction rates
ODE	calculated using one-dimensional equilibrium computer program
ODK	calculated using one-dimensional kinetic computer program
(O/F)avg	corresponding to overall average mixture ratio
(O/F)dist	effects due to mixture-ratio distribution
pred	analytical prediction of experimental value
HL	effects due to heat lost to injector face and to chamber wall upstream of boundary-layer attachment point
rad	radiation effect
TDK	calculated using two-dimensional kinetic computer program
vap	corresponding to local evaporated mass or mixture ratio
x	axial position in thrust chamber
ϵ	corresponding to the nozzle exit-area ratio
ϵ'	corresponding to the equivalent inviscid-flow nozzle area ratio
2D	two-dimensional flow effects

REFERENCES

1. Pieper, J. L., ICRPG Liquid Propellant Thrust Chamber Performance Evaluation Manual, CPIA Publication No. 178, AD 843 051, Aerojet-General Corporation, prepared for the ICRPG Performance Standardization Working Group, Sept. 30, 1968.
2. Kors, D. L., Bassham, L. B., and Walker, R. E., "A Liquid Rocket Performance Model Based on Vaporization Interactions," J. Spacecraft and Rockets, Vol. 6, No. 10, pp. 1133-1138, Oct. 1969.
3. Back, L. H., and Cuffel, R. F., "Flow Coefficients for Supersonic Nozzles With Comparatively Small Radius of Curvature Throats," J. Spacecraft and Rockets, Vol. 8, No. 2, pp. 196-198, Feb. 1971.
4. Hoehn, F. W., Predicted Stagnation Pressure for Characteristic Velocity Measurement, Jet Propulsion Laboratory, Pasadena, Calif. (to be published).